



Optimization of electric vehicle sound package based on LSTM with an adaptive learning rate forest and multiple-level multiple-object method

Haibo Huang ^{a,c}, Xiaorong Huang ^b, Weiping Ding ^{a,*}, Siwen Zhang ^{c,d}, Jian Pang ^{c,d,*}

^a School of Mechanical Engineering, Southwest Jiaotong University, 610031 Cheng Du, Si Chuan, China

^b Vehicle Measurement, Control and Safety Key Laboratory of Sichuan Province, Chengdu 610039, China

^c State Key Laboratory of Vehicle Noise, Vibration and Harshness (NVH) and Safety Technology, 401120 Chongqing, China

^d Changan Auto Global R&D Center, Chongqing Changan Automobile Co., Ltd, 401120 Chongqing, China



ARTICLE INFO

Communicated by Kihong Shin

Keywords:

Noise, vibration and harshness
Acoustic package
Knowledge- and data-driven
Long short-term memory
Multiple-level multiple-object

ABSTRACT

The sound absorption and sound insulation performance of an acoustic package (AP) system directly affect the noise, vibration and harshness performance of a vehicle. Numerous studies have studied the optimization of vehicle sound package, however, there are two deficiencies in the current research of sound package: (1) The noise transmission path of acoustic package is complex and hierarchical. Most of the related works focus on the data-driven part while ignoring the knowledge attributes behind the acoustic package design problem, which limits the further improvement of prediction and optimization of acoustic package performance. (2) In using intelligent neural networks-based methods such as long short-term memory (LSTM), reducing the learning rate during training gradually narrows the search interval of a solution, and adjusting the learning rate in a small range may tend to trap local optima. In this study, a knowledge- and data-driven approach is proposed for the development of acoustic package systems. A multiple-level multiple-object method is proposed as the knowledge model, and a multilayer structure of the acoustic package system that contains the system, subsystem and component layers is developed. In addition, an improved long short-term memory model based on an adaptive learning rate forest, which can increase and decrease the learning rate adaptively, is proposed as the data-driven model. The knowledge- and data-driven method is applied to optimize the sound absorption and insulation of the acoustic package system. In the experimental validation, the effectiveness and robustness of the proposed method outperformed the traditional direct mapping method and the conventional long short-term memory method.

1. Introduction

With the increasing awareness of environmental protection and the popularization of electric vehicles (EVs), the overall interior noise has gradually decreased, while the requirements of consumers for vehicle sound quality have gradually increased. The acoustic

* Corresponding authors at: School of Mechanical Engineering, Southwest Jiaotong University, 610031 Cheng Du, Si Chuan, China (W. Ding), State Key Laboratory of Vehicle Noise, Vibration and Harshness (NVH) and Safety Technology, 401120 Chongqing, China (J. Pang).

E-mail addresses: huanghaibo214@swjtu.edu.cn (H. Huang), huangxiaorong@mail.uc.edu (X. Huang), dwp@swjtu.edu.cn (W. Ding), zhangsw@changan.com.cn (S. Zhang), pangjian@changan.com.cn (J. Pang).

package (AP) is a key system to improve the noise, vibration and harshness (NVH) performance of EVs, and it has become a crucial focus of technology and product competition [1,2]. A vehicle AP refers to a combination of acoustic components that reduce the sound pressure of the air in a car and have an important influence on the distribution of interior acoustic characteristics [3]. The front wall, floor, dashboard and trunk are the main components of the entire acoustic package, and their sound absorption and insulation (SAI) abilities directly affect the vehicle's NVH performance [4]. A well-designed acoustic package can reduce the noise level and improve the acoustic quality of the car as well as promote a light weight and reduce the cost of the vehicle. Therefore, research on improving the performance of vehicle acoustic packages has important practical and engineering significance.

Previously, due to technical limitations (finite element and its derivative methods have low accuracy in the calculation of mid- and high-frequency noise), the design and development of automotive acoustic packages were mainly based on actual prototype cars and compared with standard cars through experiments [5]. Zhang et al. [6] studied the structure-acoustic coupling mechanism between two adjacent flexible panels and an enclosed cavity based on modal expansion methods. With the development and engineering of statistical energy analysis (SEA) theory and the promotion of large-scale commercial software such as VA One [7], the analysis of mid- and high-frequency noise in the car has been improved. Lee et al. [8] established an EV model based on the SEA method, analyzed the contribution of sound transmission losses of an AP and optimized the weight of the dash. Thompson et al. [9,10] used the SEA and hybrid FE-SEA methods to predict the airborne noise and structure-borne noise inside railway vehicles. A vehicle AP model based on a deterministic and SEA method was developed by Mohamed et al. [11] to analyze the tire noise transmission characteristics. The effectiveness of the SEA method in acoustic package engineering design is undoubtedly. However, it is difficult to obtain accurate values of acoustic package material parameters (such as the porosity, viscous characteristic length, thermal characteristic length, etc.) and characteristic parameters (such as the modal density, internal loss factor, coupling loss factor, etc.) that are required to construct the SEA model. As a result, the SEA-based simulation model needs to be simplified and adjusted, and the simulation results are mainly comparable with the test results in specific working conditions and the model confidence is not good in other working conditions.

Although accurate acoustic package material and characteristic parameters are difficult to obtain, the SAI test performance and the thickness and area of the acoustic package are relatively easy to determine. In the era of big data and intelligence, data-driven methods provide more technical means for the development of vehicle acoustic packages. They can substitute the precise derivation between acoustic and vibration mechanics by using the fuzzy mapping relationship between easily obtained test data to guide the forward development of the acoustic package. Yu et al. [12] used the material and thickness of the vehicle firewall as design parameters and the interior sound pressure level as the design target; an approximate model was developed based on the kriging method, and the prediction accuracy reached 0.92. In [13], a convolutional neural network (CNN) model was applied to analyze the weight and cost of floor panels; without weakening the original SAI performance of the AP, the total weight and cost of floor panels were reduced by 12.1 % and 6.7 %, respectively. Nam et al. [14] employed a CNN and long short-term memory (LSTM) networks to classify the impact noise in a vehicle and found that the interior sound has the characteristic of long-range correlation, which is more suitable for analysis with the LSTM model. Hannan et al. [15] improved the LSTM with a learning rate-optimized method, which achieved a high regression accuracy in estimating the state-of-charge of vehicle batteries. However, for a data-driven model, the prediction accuracy can be compared to the accuracy of the simulation model. Traditional shallow networks have a limited ability to fit complex problems, while advanced deep networks are sensitive to model hyperparameters. Therefore, to obtain accurate AP prediction results, it is necessary to improve the prediction performance of the LSTM model.

In general, most NN-based methods use stochastic gradient descent for parameter updating, in which the learning rate is crucial for model training. This is because a high learning rate increases loss error and results in excessive changes in weight; a low learning rate can prevent these problems but increases convergence time. An effective method for avoiding this problem is to reduce the learning rate during training. The three most popular methods for adaptive learning rates are AdaGrad, RMSProp and Adam [16], which gradually narrow the learning rate in the parameter updating process. However, these methods rely heavily on the initial learning rate, and this problem influences the performance of NN-based methods. Therefore, a good training strategy for parameter updating is crucial to obtain preferable results. Schaul et al. [17] proposed a method of automatically adjusting multiple learning rates to minimize expected errors at any time but it requires many extra calculations. In [18], a dynamic adjustment strategy of the learning rate was developed based on the LSTM model and the gradients of the loss function, which obtained relatively good results. However, a problem still exists: if the search range for a solution changes slightly, searching for a better solution becomes difficult. Although a state-of-the-art learning rate updating method based on the multistep tree was developed in [19], the updating strategy may be trapped in local minima. Therefore, a more effective learning rate updating method is expected.

In practice, the noise transmission path of an AP is complex, and the amount of valid test data is small. Direct construction of a data-driven model between the design parameters (material, thickness, area, etc.) and the AP performance may have the risk of underfitting because the overall AP performance is weakly related to the design parameters while highly correlated to the transmission loss and insertion loss of components and transfer paths [20]. Huang et al. [21] noted that the acoustic package covers many levels of performance at the vehicle level, system level and component level, and involves structural parameter matching. This makes the design of acoustic packages exhibit a complex hierarchy in physical structure and noise signal transmission. Ambardekar et al. [22] found that the vehicle component parameters have uncertainties and correlations, and that changing the parameter from its own targets may not favorably influence vehicle-level NVH performance but may benefit system-level NVH performance due to multiple excitations from tire/road, wind and power-train noise sources. In fact, without considering the SAI characteristics of systems and transfer paths, the complexity of the correlation between the design parameters and the AP target increases dramatically, which affects the prediction accuracy [23]. Bergen et al. [24] improved the mid-frequency acoustic performance of an AP using a target set process based on transfer path analysis and panel contribution analysis techniques. The knowledge-based method that introduces a noise transmission path and target programming can reduce the complexity and nonlinearity of the problem and alleviate the issue of insufficient effective

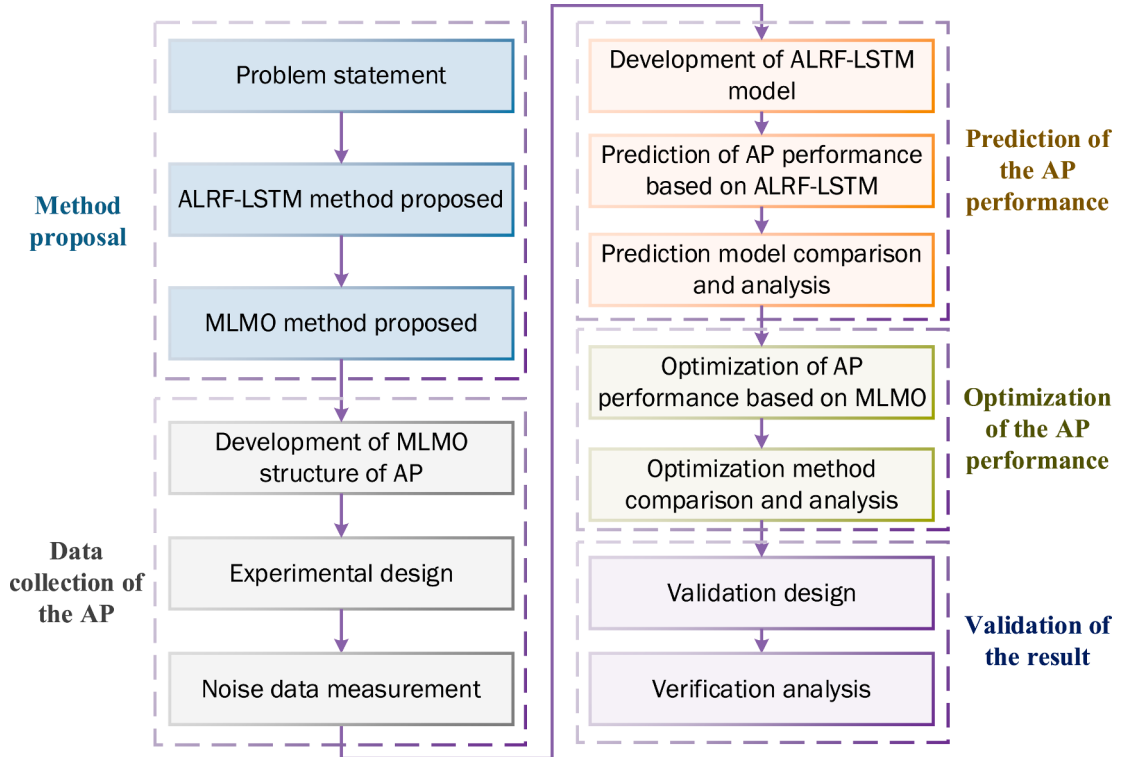


Fig. 1. Process of prediction and optimization of the AP performance of an EV.

data. Therefore, combining data-driven and knowledge-based methods is essential and urgent in developing and optimizing the performance of vehicle APs.

Based on the above analysis, many studies have been performed to analyze and improve the AP performance of EVs and have achieved effective results. However, the following problems remain in the development of the AP:

- (1) In using intelligent NN-based methods such as LSTM, reducing the learning rate during training gradually narrows the search interval of a solution, and adjusting the learning rate in a small range may tend to trap local optima. A new parameter updating method is necessary to improve the training performance of LSTM.
- (2) The noise transmission path of AP is complex and hierarchical. Most of the related works [12–24] focus on the data-driven part while ignoring the knowledge attributes behind the AP design problem, which limits the further improvement of prediction and optimization of AP performance. It is beneficial to combine data-driven methods and knowledge-based approaches for AP development.

Consequently, an improved LSTM model based on adaptive learning rate forest (ALRF-LSTM) is proposed, and a multiple-level multiple-object (MLMO) structure of an AP for EVs is presented to solve the aforementioned problems. There are two original contributions of this paper: 1) ALRF-LSTM is able to decrease and increase the learning rate adaptively in accordance with the training loss and can obtain a better solution through a large search range of the learning rate. 2) the proposed MLMO structure can reduce the complexity of the problem via the decomposition of the system, subsystem, and component levels, thereby improving the prediction and optimization effectiveness of the AP.

This paper is organized as follows. In [Section 2](#), the process of prediction and optimization of AP performance is presented. In [Section 3](#), the ALRF-LSTM method and MLMO structure are introduced and proposed. In [Section 4](#), the AP experiment and test of an EV are described, and the data analysis work is presented. In [Section 5](#), the performance of AP is predicted, optimized and validated through the proposed methods. Finally, [Section 6](#) summarizes the conclusion of this paper.

2. Prediction and optimization of AP performance

The process of prediction and optimization of AP performance using the ALRF-LSTM and MLMO methods in this paper is presented in [Fig. 1](#) and comprises the following five steps.

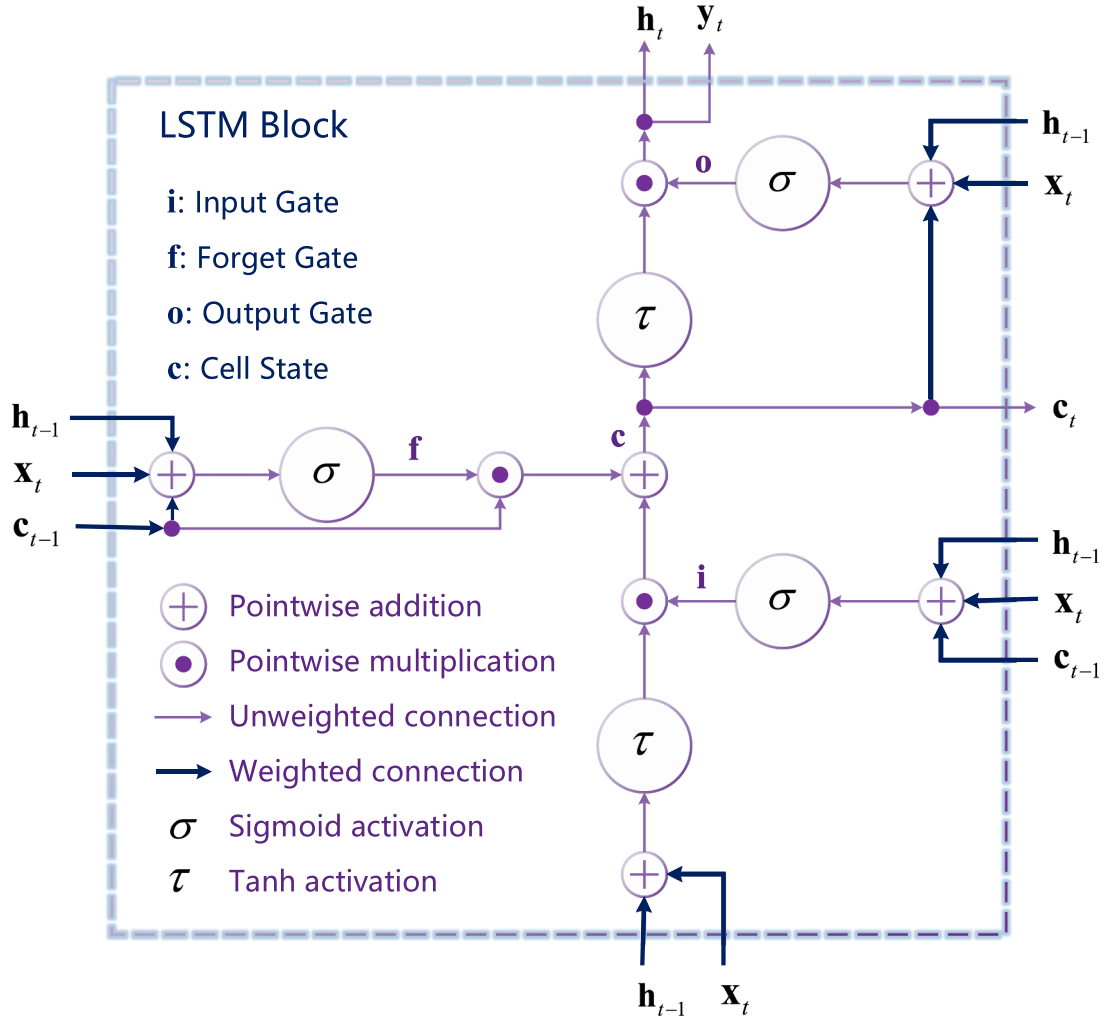


Fig. 2. The LSTM block.

- (1) The drawback of the conventional LSTM method is illustrated, and the improved ALRF-LSTM method and its calculation process are proposed. In addition, to reduce the complexity of the problem and improve the prediction accuracy, the MLMO design method, which combines data-driven methods and knowledge-based approaches for AP development, is proposed.
- (2) According to the MLMO design method, the MIMO structure of an AP is developed. Experiments for noise collection are designed using the wave tube, sound absorption room, reverberation room, and reverberation room-anechoic room. The sound translation loss (STL) and sound isolation loss (SIL) [25] of the AP system, subsystem and components are recorded and analyzed.
- (3) The prediction model of AP performance based on the ALRF-LSTM is developed, which uses the SIL of AP components as inputs. The STL and SIL of the AP system and subsystems are used as hierarchical outputs. The accuracy of ALRF-LSTM is analyzed using different model parameters, and the performance of the prediction method is compared with other conventional methods.
- (4) To reduce the EV interior noise and improve the noise experience, the parameters of AP are optimized hierarchically through the MLMO structure and the GA method. The nonlinearity of the AP system is decomposed into several submodels, which decreases the computational complexity. The optimization result based on the MLMO method is analyzed and compared with the conventional optimization method.
- (5) The accuracy and effectiveness of the optimization performance of the proposed method is verified and analyzed through an in situ vehicle experiment.

3. The proposed method

3.1. LSTM based on adaptive learning rate forest (ALRF-LSTM)

3.1.1. Brief introduction of LSTM

The LSTM model is a variant of the recurrent neural network (RNN), which uses a special memory cell to represent the long-term dependencies in series data [26]. Similar to traditional neural networks that have neurons, LSTM networks have LSTM blocks that are connected through successive layers. These nonlinear blocks learn to open or close gates in the network to regulate the error flow [27]. The key in the LSTM block is the cell state, which resembles a conveyor belt. It runs straight down the entire chain with the ability to add or remove information to the cell state, and is regulated through different gates called the input gate, forget gate, and output gate [28].

As shown in Fig. 2, an LSTM block receives an input sequence, and then each gate uses activation units to decide whether they are triggered or not. This operation makes the change of state and addition of information that flows through the block conditional [29]. The gates have weights that can be learned during the training phase. LSTM is trained through backpropagation through time, and it can overcome the vanishing gradient problem.

Given an input x_t at time step t and the hidden state \mathbf{h}_{t-1} from the previous time step, the input gate i_t , forget gate f_t , cell state c_t , output gate o_t , and output y_t can be computed via Eq. (1). The output y_t is used as the hidden state \mathbf{h}_t in the next time step.

$$\begin{aligned} i_t &= \sigma(W_{xi}x_t + W_{hi}\mathbf{h}_{t-1} + W_{ci}c_{t-1} + b_i) \\ f_t &= \sigma(W_{xf}x_t + W_{hf}\mathbf{h}_{t-1} + W_{cf}c_{t-1} + b_f) \\ c_t &= f_t c_{t-1} + i_t \tanh(W_{xc}x_t + W_{hc}\mathbf{h}_{t-1} + b_c) \\ o_t &= \sigma(W_{xo}x_t + W_{ho}\mathbf{h}_{t-1} + W_{co}c_{t-1} + b_o) \\ y_t &= \mathbf{h}_t = o_t \tanh(c_t) \end{aligned} \quad (1)$$

where w_{xi} , w_{xf} , w_{xc} , and w_{xo} are input weights; w_{hi} , w_{hf} , w_{hc} , w_{ho} , w_{ci} , w_{cf} , and w_{co} are recurrent weights; and b_i , b_f , b_c , and b_o are biases.

Stochastic gradient descent is a widely used updating approach in LSTM. The parameter updating is performed for each sample or for each mini batch:

$$\theta_{t+1} = \theta_t - \eta \cdot \nabla_{\theta_t} E(\theta_t; x^{(i)}; y^{(i)}) \quad (2)$$

where θ are the weights or biases, $x^{(i)}$ is the input with training sample i , $y^{(i)}$ is the i th label, E is the loss function, and η is the learning rate. Increasing η could expand the search range and avoid local optima; however, a large η makes the calculation difficult to converge. An effective way to avoid this problem is to reduce the learning rate gradually during training. The stepwise learning rate approach, which reduces η to 10 % of its original value, is a convenient method to adjust the learning rate. In addition, newly developed updating methods, such as AdaGrad and Adam, can adaptively adjust the learning rate through the parameter gradient.

3.1.2. The drawback of LSTM and the proposed ALRF-LSTM

Most LSTM updating methods, such as AdaGrad and its derivative methods, are designed to decrease during training to balance the convergence and computing time. However, the narrowing of the search range gradually makes it difficult to search for a better solution and it can easily become trapped in a local minimum. In contrast, increasing the learning rate can expand the search range and avoid pooling local solutions, which makes convergence difficult. Therefore, to overcome this drawback, a more flexible updating method for the learning rate, ALRF, which combines adaptive decreases and increases in the learning rate in the training process, is proposed to improve the accuracy of LSTM.

The purpose of the training is to minimize the loss function, and we prefer to obtain a smaller training loss. Therefore, the ALRF approach performs training independently and in parallel with several learning rates and selects the learning rate that results in the smallest training loss during each epoch. For regression problems, the mean squared error (MSE) is commonly used as the loss function, and the cross-entropy is commonly used for classification problems. In this study, we choose the half mean squared error as the regression loss function, which is defined as follows:

$$Loss = \frac{1}{2P} \sum_{i=1}^P (x_i - y_i)^2 \quad (3)$$

where P is the number of training samples, x_i is the actual output of unit i , and y_i is the target output of unit i .

To develop the ALRF-LSTM, a forest structure with 4 epochs is introduced to represent the state transition in the learning process, as shown in Fig. 2. The nodes represent the model states during training, and the arrows represent the state transitions using different learning rates. There are three hyperparameters in ALRF-LSTM: the branch size, the scale factor, and the beam space. The branch size is defined as the feasible range that can be searched. The scale factor is the coefficient used to tune the learning rate in each epoch. The beam space represents the bounded width of the potential optima solution. The training procedure is performed as follows:

Step 1: The branch size (U), the scale factor (S), and the beam space (V) are predefined. The branch size and the scale factor are consistent for each node, and the beam space is consistent for each epoch.

Step 2: In epochs 1 → 2, the training is performed in parallel with different scale factors, and the learning rate in each branch (given $U = 5$) is calculated via Eq. (3). The training losses of all branches in this epoch are sorted in ascending order. The nodes with the top V

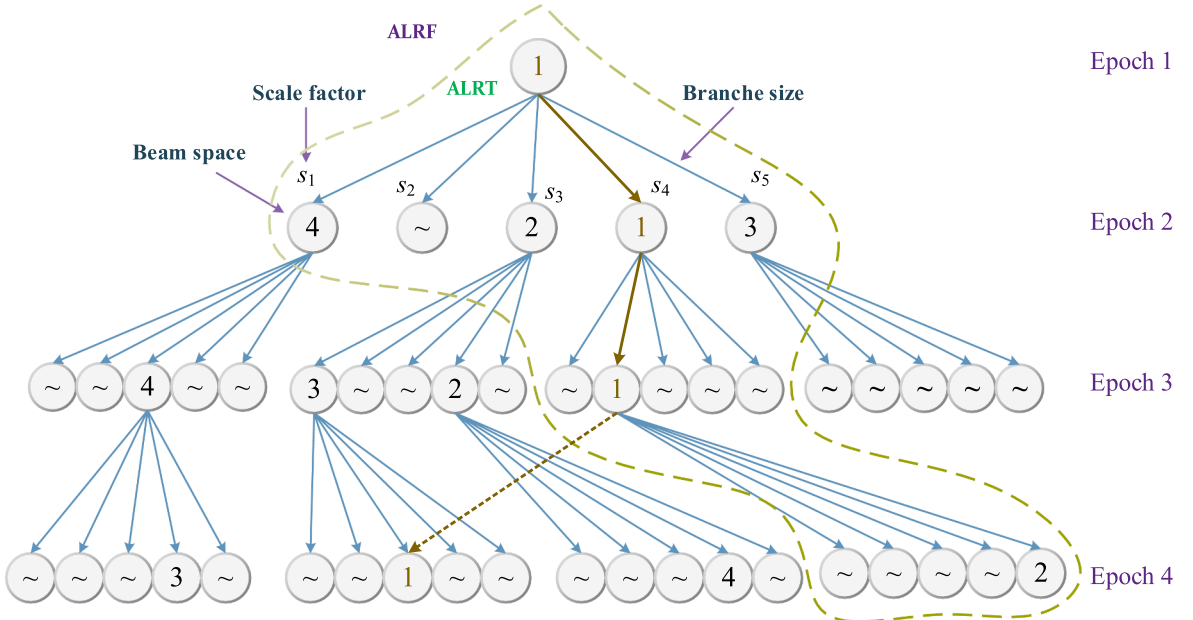


Fig. 3. Structure of LSTM with an adaptable learning rate forest.

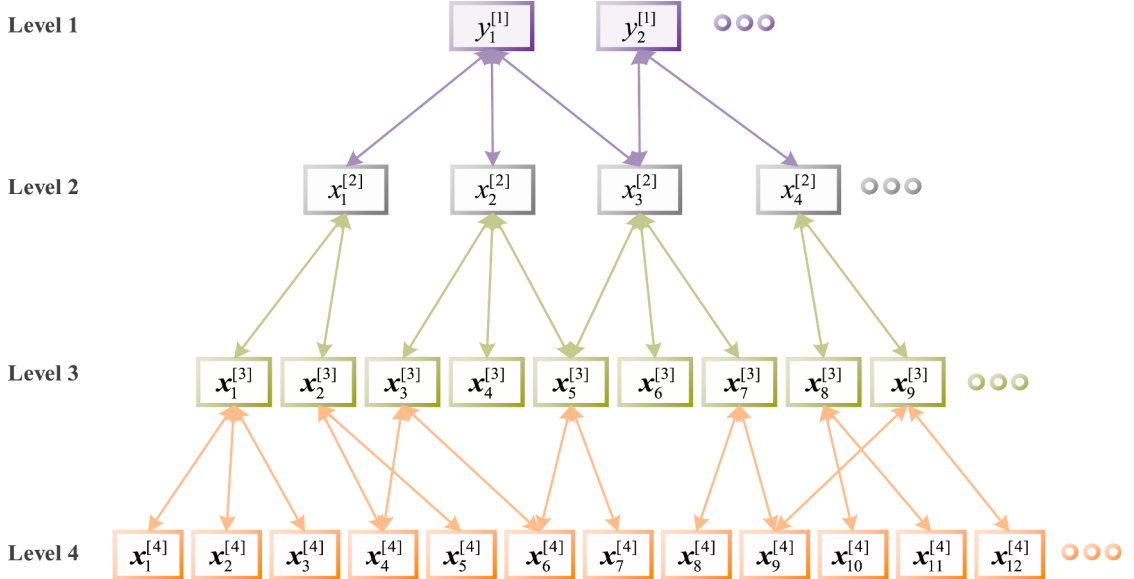


Fig. 4. Schematic of the MLMO architecture.

(given $V = 4$) training loss are stored as candidates for the next step, and the remaining node is eliminated.

$$\eta_{h+1} = \eta_h \cdot S_{t_h} \quad (4)$$

where η_h is the learning rate at epoch h (here, $h = 1$) and S_{t_h} is the t -th scale factor (here, $t_h = 4$).

Step 3: In epochs 2 → 3, through independent and parallel training, the 4 candidates in epoch 2 generate 16 candidates in epoch 3. The 4 nodes with the lowest training loss are stored, and the remaining 12 nodes are eliminated.

Step 4: In epochs 3 → 4, training is performed as in the previous epoch, and the 4 nodes with the smallest training loss are stored. The learning rate at epoch H can be calculated via Eq. (4). The state transmission is shown by the bold line in Fig. 3, which indicates that the lowest training loss is not always in one tree route. The multiple branches and beams form a forest so that the state transition can jump through different tree routes. This characteristic can avoid local optima and obtain a better solution.

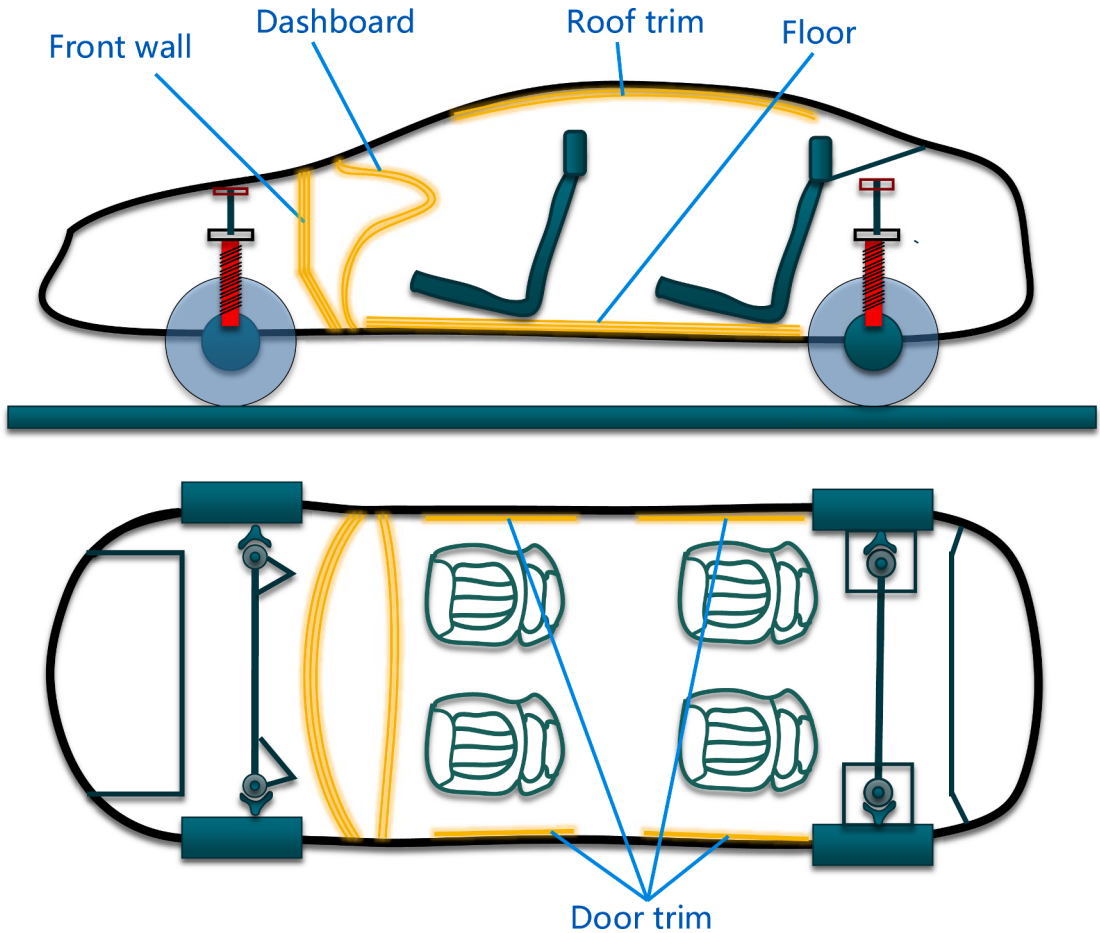


Fig. 5. The AP system and subsystems of the tested EV.

$$\eta_H = \eta_0 \cdot \prod_{h=1}^{H-1} S_{t_h} \quad (5)$$

where η_0 is the initial learning rate.

Step 5: In epoch 4→~, training is continued according to step 2 to step 4 until the stop condition (for instance, the maximum iteration number or the minimum training loss has been researched) is achieved.

The calculation accuracy and efficiency are controlled by the branch size, beam space, and scale factor. Increasing the branch size and beam space expands the number of routes that can be searched but increases the computational time. However, the parallel computation for training at each epoch can solve this problem [30]. In addition, an appropriate composition of the scale factor is beneficial to improve the training accuracy. If the beam space is set to 1, the ALRF would turn out to be the adaptive learning rate tree (ALRT) [19], which is shown within the dashed line in Fig. 3, and the training time would be effectively reduced. Although the ALRT may miss the global optima, it still has advantages compared to the conventional method.

3.2. The multiple-level multiple-object (MLMO) method

The performance of an AP, which is reflected in the interior SPL of EVs, is explicit to the driver and passenger while implicit to its influencing factors. This is because the AP is not a completely independent system but consists of many subsystems and components. Therefore, optimizing the AP performance cannot be limited to the two levels of the surface system property and basic component property but needs to analyze the subsystem properties that are distributed between the system and component levels. Based on this concept, a hierarchical analysis method, MLMO architecture, is developed in this paper, as shown in Fig. 4. The relative lower-level variables must meet the requirement of relative higher-level objectives and ultimately satisfy the top-level design objectives. The higher-level objectives are “shared” by multiple design objectives in the lower level that are connected to them. This leads to a game of goals between and within the hierarchy. The MLMO architecture shown in Fig. 4 has two advantages: 1) gradient decomposition of objectives and variables according to levels is beneficial to reduce the design difficulty and conform to the engineering development

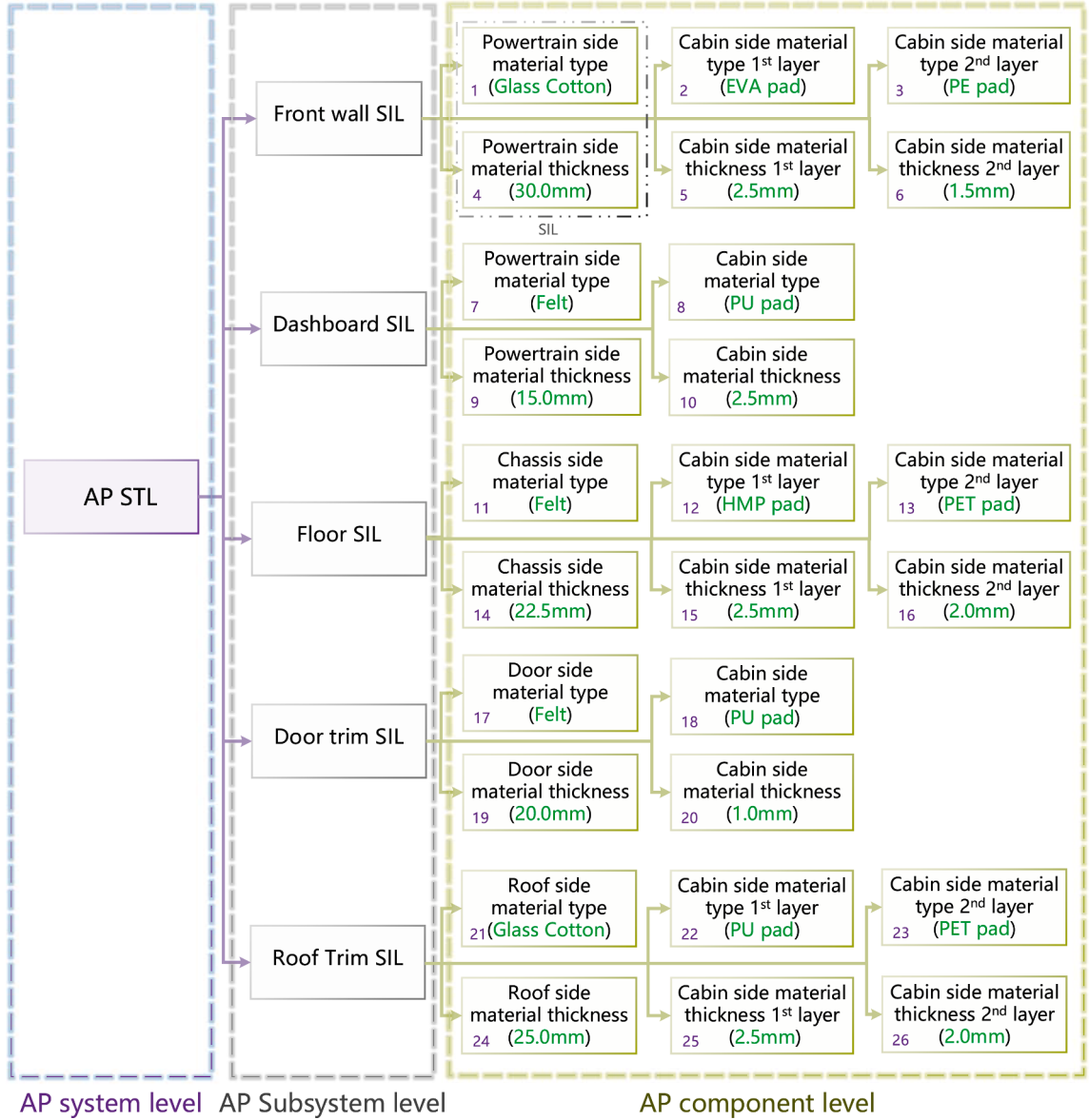


Fig. 6. The MLMO structure of the AP of the tested EV. (The subscript number representatives the corresponding component parameter in the box; and the EVA, PE, PU, HMP, PET are sound absorption and insulation materials, whose full name are listed in Appendix A).

process; 2) the existence of the intermediate layer (such as subsystem layers) reduces the nonlinearity and complexity of the entire model, making it easier to avoid local optimal solutions.

Based on the MLMO architecture, the numerical model for hierarchical prediction and optimization can be established as follows:

$$\begin{aligned}
 & \min \{y_k^{[l]}\}, \quad k = 1, 2, \dots, K \\
 & y_k^{[l]} = f_k^{[l]}(x_1^{[l+1]}, x_2^{[l+1]}, \dots, x_I^{[l+1]}), \quad l = 1, 2, \dots, L \\
 & \text{s. t.} \quad h_m^{[l]}(x^{[l]}) = 0, \quad m = 1, 2, \dots, M \\
 & g_n^{[l]}(x^{[l]}) \leq 0, \quad n = 1, 2, \dots, N \\
 & \text{var.} \quad x_i^{[l+1]} \in \mathbf{L}_n^{[l+1]}, \quad i = 1, 2, \dots, I \\
 & \quad y_k^{[l]} \in \mathbf{L}_k^{[l]}, \quad k = 1, 2, \dots, K
 \end{aligned} \tag{6}$$

where L is the total number of levels in the MLMO structure and l is the computation level. $y_k, k = 1, 2, \dots, K$ is the design objective of the adjacent higher level, and K is the number of objectives of this level. $x_i, i = 1, 2, \dots, I$ is the design variable of the adjacent lower level, and I is the number of variables of this level. f_k is the prediction model, which is used to map the relationship between the design

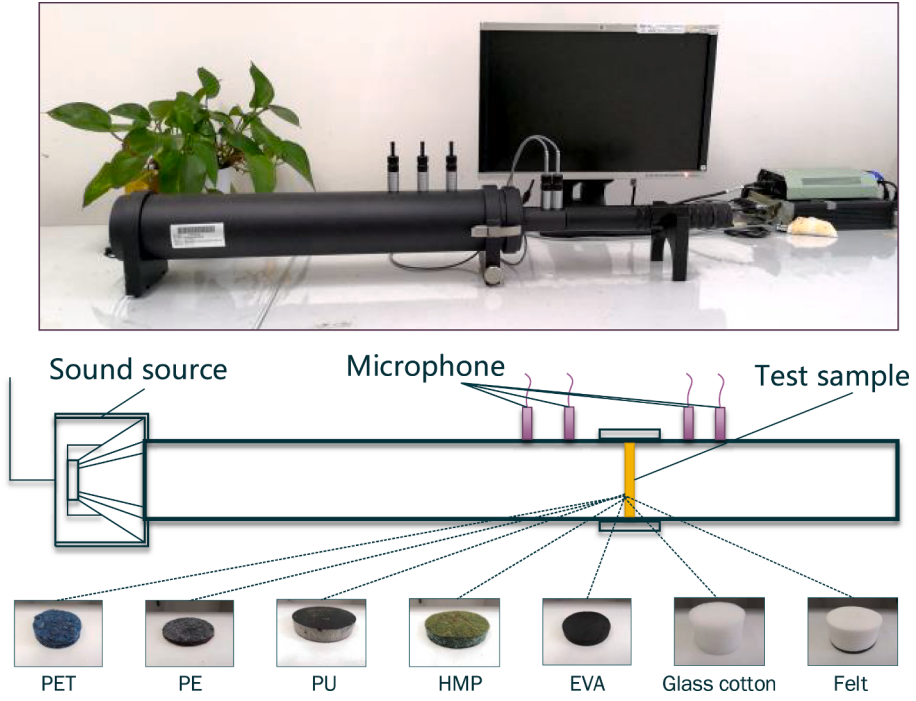


Fig. 7. The SIL test of AP components using the wave tube.

variables and design objectives. Therefore, the accuracy of f_k is critical to the effectiveness of the prediction and optimization results, and the proposed ALRF-LSTM is selected as the f_k . h_m and g_n are constraints. Due to the decomposition of MLMO, the whole prediction model can be regarded as the prediction process of forward hierarchical transfer, while the optimization model can be regarded as the optimization process of reverse hierarchical transfer, which is different from the classic prediction and optimization model.

4. Experiment and test of the AP

4.1. Development of the MLMO structure of the AP

A real vehicle, a CHANGAN CS55 EV, which provided by the Changan Auto Global R&D Center, Chongqing Changan Automobile Co., Ltd, Chongqing, China, was used for the analysis. According to the distribution of SAI materials, the AP system can be decomposed into five main subsystems: the front wall, dashboard, floor, door trim, and roof trim, as shown in Fig. 5. The SIL of these subsystems affect the interior AP STL of the EV. Therefore, the AP STL is regarded as the objective of the system level, and the SIL of the front wall, dashboard, floor, door trim, and roof trim are regarded as the objectives of the subsystem level. Furthermore, the SIL of each subsystem is affected by its component properties. For instance, the front wall consists of three layers of SAI components (one layer on the powertrain side and two layers on the cabin side), which are EVA, PE, and felt material types with 2.5 mm, 1.5 mm, and 30.0 mm thicknesses, respectively; the dashboard consists of two layers of SAI components (one layer on the powertrain side and the other layer on the cabin side), which are EVA and felt material types with 2.5 mm and 10.0 mm thicknesses, respectively. Similarly, the rest of the AP subsystems can be decomposed into different material types and thicknesses. The MLMO structure of the AP of the tested EV was established, and is shown in Fig. 6.

4.2. Experiment and analysis

According to the developed MLMO structure of the AP, the noise data were measured and analyzed. The SAI materials are the base parts of the AP components, and thus an acoustical properties database was developed. Based on the standard ISO 10534–2 [31], the SILs of each material (EVA pad, PE pad, PU pad, HMP pad, felt and glass cotton) were measured and calculated through the wave tube. The thicknesses of the EVA pad, PE pad, PU pad, HMP pad were 1.0 mm to 10.0 mm, with an interval of 0.5 mm, and the thicknesses of the felt and glass cotton were 5.0 mm to 40.0 mm, with an interval of 2.5 mm. The tested material size was a circle with a diameter of 100 mm. In the experiment, G.R.A.S. 40 HF2 microphones were used to record the noise with a sampling rate of 48 kHz. A Siemens LMS data acquisition system was used to collect the data. The mounting positions of the microphones and SAI materials are shown in Fig. 7. The calculation process of SIL in the wave tube is presented in [32].

The functions of the front wall, dashboard, floor, door trim, and roof trim are to absorb and isolate the vehicle noise; therefore, the SILs of these subsystems were measured through the reverberation room-anechoic room [33]. According to the standard SAE J1400

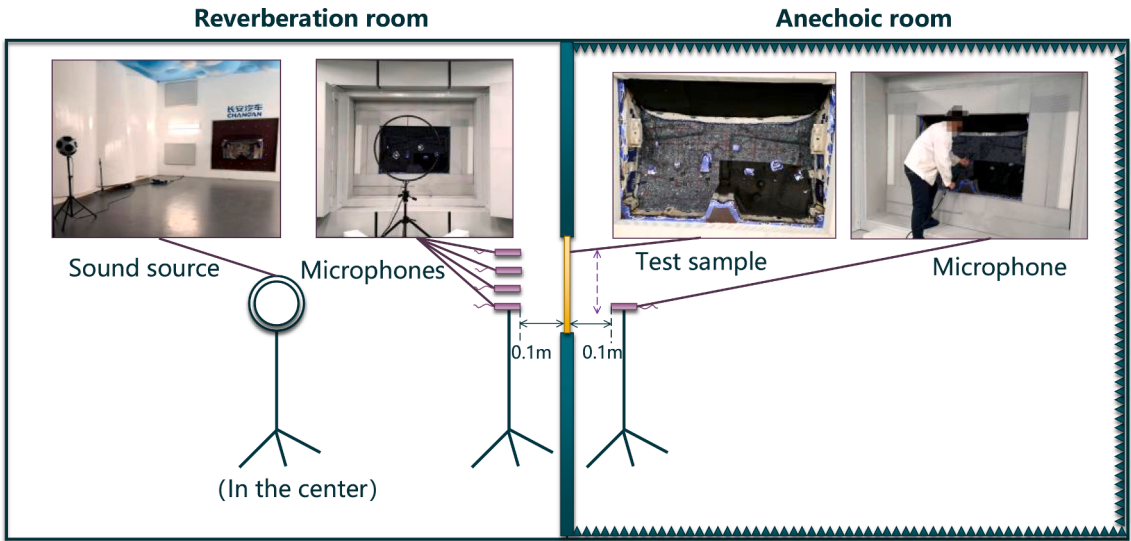


Fig. 8. The SIL test for AP subsystems using the reverberation room-anechoic room.

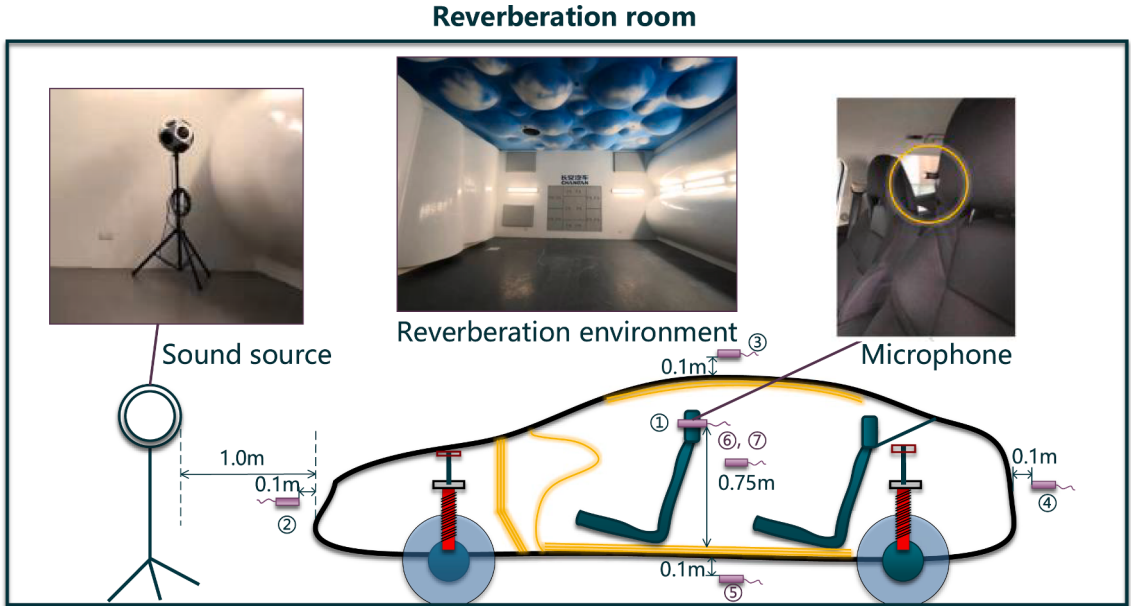


Fig. 9. The STL test of AP system using the reverberation room.

[34], the test sample was mounted on the middle wall in the reverberation room-anechoic room, and a fixture and sealing putty were used to prevent noise leakage. The dodecahedron spherical sound source was placed on the center of the reverberation room to generate random noise with an overall SPL of 120 dB. Four microphones were placed 0.1 m from the front of the test sample in the reverberation room, and their averaged SPL was calculated. In addition, one microphone was arranged 0.1 m from the rear of the test sample in the anechoic room. The microphone was moved in a rectangular path to record the averaged SPL after sound absorption and insulation by the test sample. The arrangement of microphones and the test sample are shown in Fig. 8. The background noise of the anechoic room was 30 dB. With the test sample installed on the middle wall, the background noise at the microphone place in the reverberation room was 20 dB lower than that at the sound source place. The SIL of the test sample can be calculated through the SPL measured before and after the sample installation [26].

The STL of the AP system was measured to reflect its performance. The tested AP system was arranged on the EV, which was parked in the reverberation room. Following the experimental method in the standard GB/T 18,697 [35], to collect interior noise, a microphone was mounted on the driver's seat near the right ear of the driver (①), 0.25 m away from the centerline of the seat at a height of 0.75 m, as shown in Fig. 9. According to the standard GB/T 6881.2 [36], to collect the near-field noise around the vehicle, five

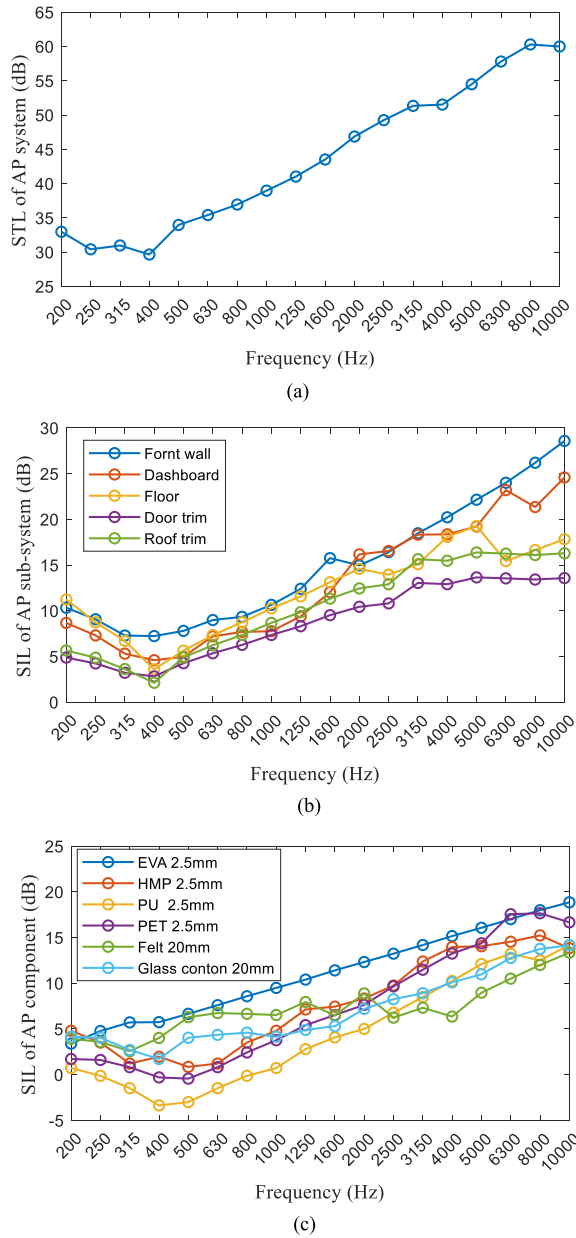


Fig. 10. The tested STL and SIL of the AP. (a) STL of the AP system, (B) SILs of the AP subsystems, (c) SILs of the AP components.

microphones were placed immediately ahead (②), immediately above (③), directly behind (④), directly below (⑤), and between the two sides (⑥, ⑦) of the vehicle at a distance of 0.1 m. The dodecahedron spherical sound source was placed 1 m from the front of the EV. Random noise was generated with an overall SPL of 120 dB. In the vehicle test, only a recorder was seated in the cabin; the powertrain and the air conditioning system were turned off, and all the windows were closed. The STL of the AP in the vehicle test can be calculated using the interior SPL and the averaged SPL outside the EV [37]. Fig. 10 shows the partially tested STL and SIL of the AP system, subsystems and components.

To collect sufficient data for analysis, several AP statuses of the tested EV were arranged. The SILs of components in the MLMO structure were selected as the design parameters, which are related to the component material type and thickness. The design of the experiment was applied to guide the AP subsystem and system experiments. For each AP subsystem, the Latin hypercube design (LHD) method [38,39] was adopted. The design factors were the material type and thickness of the components in different layers. The design levels for the material type and thickness were as follows: the EVA pad, PE pad, PU pad, and HMP pad are interchangeable, and the felt and glass cotton are interchangeable. The thickness range of the EVA pad, PE pad, PU pad, and HMP pad was 1.0 mm to 5.0 mm, with an interval of 0.5 mm, and the thickness range of the felt and glass cotton was 5.0 mm to 40.0 mm, with an interval of 2.5 mm. Fifty

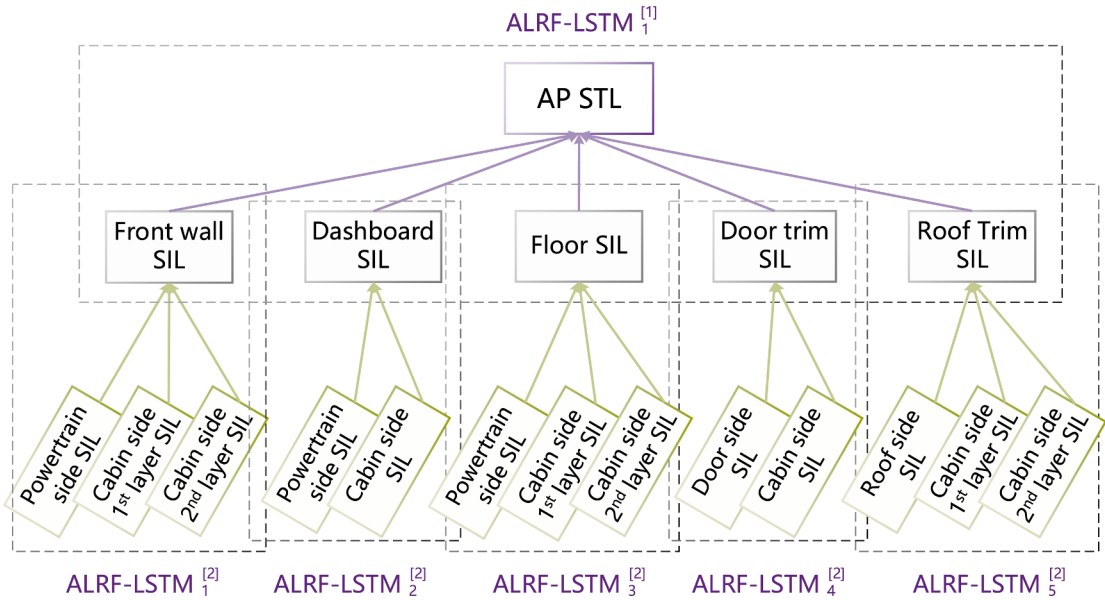


Fig. 11. AP prediction model based on MLMO and ALRF-LSTM.

sample seeds based on the design factors and levels for each AP subsystem were generated. During the experiment, the AP subsystem samples were assembled based on the LHD combination and then measured independently in the reverberation room-anechoic room. Therefore, 50 tests for each AP subsystem were implemented, and a total of 250 SILs of AP subsystems were obtained. Similarly, the LHD method was used for the AP system experiment. The design factors were the five AP subsystems, and the design levels for each AP subsystem were the 50 SILs tested above. Fifty sample seeds based on the design factors and levels for the AP system were generated. One combination of AP systems was arranged on the EV to collect the noise inside and outside the vehicle. Then, the next combination was used to substitute the former one and implement the same test. Through the 50 tests, the STLs of the AP system combinations were obtained.

5. Results and discussion

5.1. Development of the AP prediction model based on MLMO and ALRF-LSTM

The STL and SIL of the AP system, subsystems and components are obtained through the experiment, and then an AP prediction model of EV can be developed based on the MLMO and ALRF-LSTM methods. The AP performance comprises complex and nonlinear noise characteristics; therefore, several ALRF-LSTM submodels are introduced to build local mapping relationships in the AP system according to the constructed MLMO structure, as shown in Fig. 11. Each of the ALRF-LSTM networks is carefully developed.

We take the ALRF-LSTM^[2]₁ submodel as an example: the SIL curves of three SAI materials (related to the material type and thickness) are used as the input, and the SIL curve of the front wall is used as the output. Therefore, it is a sequence-to-sequence regression problem. The networks have one input layer with three neurons (consistent with the number of input features) and one output layer with one neuron that gives the predicted SIL of the front wall on a certain frequency band. The parameters of the hidden layer are related to the prediction accuracy and time cost, and the selection of the hidden layer is still an open issue. However, previous studies provided us with some references for designing LSTM networks [40,41]. In this study, we selected one hidden layer with 20 hidden neurons. The initial learning rate is set to 0.01, and the ALRF updating method is applied with branch size $U = 3$, scale factor $S = \{0.8, 1.0, 1.2\}$, and beam space $V = 3$. A scale factor of 1.0 is selected, which means that the learning rate can remain unchanged during training, and scale factors of 0.8 and 1.2 are selected to adaptively increase and decrease the learning. To reduce the stochastic error, the mean square error (MSE) of 20 trials is selected as the prediction error. The minimal batch size is selected as 4, and the number of epochs is set to 600. To reduce the instability of the loss function, a low dropout rate ($p = 0.2$) is used. The gradient threshold is set to 2 to prevent the gradients from exploding. We used the sigmoid function as the gate activation function and the tanh function as the state activation function, as presented in Fig. 2. A one-step ahead forecast is adopted, where the next time step ($t + 1$) is predicted.

Similarly, other submodels in the AP MLMO architecture can be developed, and the difference among them is the number of neurons in the input layer. ALRF-LSTM^[2]₃ and ALRF-LSTM^[2]₅ have the same model structure as that of ALRF-LSTM^[2]₁. The structures of ALRF-LSTM^[2]₂ and ALRF-LSTM^[2]₄ are identical and have two neurons in the input layer, and the other parameters are the same as those of ALRF-LSTM^[2]₁. The output of ALRF-LSTM^[2]₁ ~ ALRF-LSTM^[2]₅ is the input of ALRF-LSTM^[1]₁; therefore, ALRF-LSTM^[1]₁ has five neurons

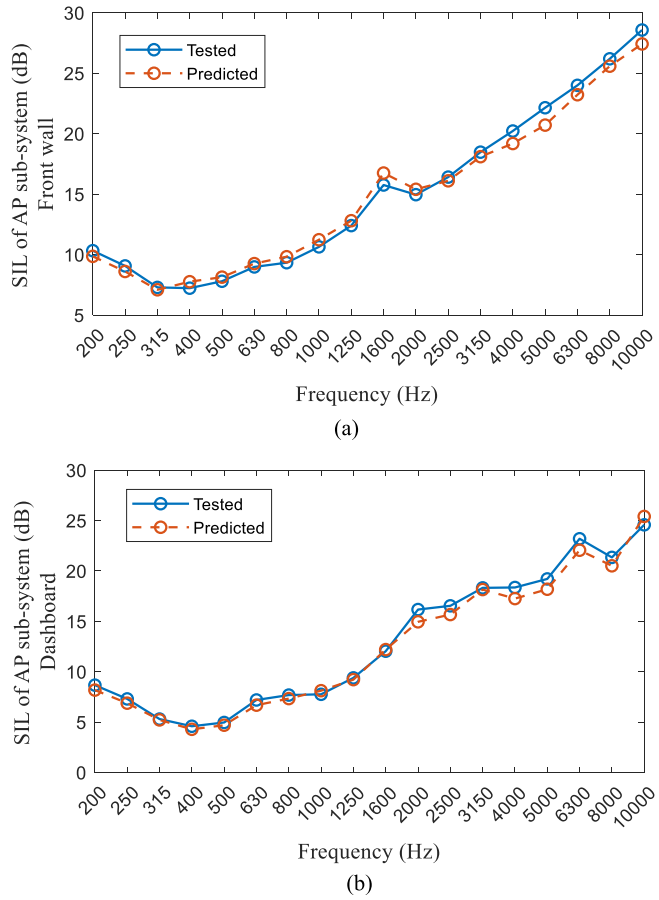


Fig. 12. The predicted SIL of the AP subsystem. (a) The front wall. (b) The dashboard.

in the input layer. These ALRF-LSTM submodels together constitute the complete AP prediction model.

In the training process, sixty samples (60 %) and forty samples (40 %) were randomly selected for training and testing the networks, respectively. The experiments were implemented using MATLAB 2022a on a workstation with an Intel(R) i7-9800X CPU and 64 GB of memory.

5.2. Prediction of AP performance

The SIL characteristics of SAI materials were obtained through the AP experiment in Section 4, and the SIL of the AP subsystems and STL of the AP systems were predicted hierarchically through the MLMO structure. Fig. 12 shows the calculation results of the ALRF-LSTM₁^[2] and ALRF-LSTM₂^[2] submodels (refer to Fig. 11 for illustration, i.e., the front wall SIL and the dashboard SIL. For the front wall SIL, the MSE and decisive factor of the predicted curve were 0.92 dB and 0.984, respectively, and the maximum and minimum relative errors for each central frequency were 5.8 % (1600 Hz) and 1.8 % (2500 Hz), respectively. In addition, for the dashboard SIL, the MSE and decisive factor of the predicted curve were 0.83 dB and 0.988, respectively, and the maximum and minimum relative errors for each central frequency were 6.4 % (400 Hz) and 1.3 % (1600 Hz), respectively. Therefore, ALRF-LSTM can predict the wideband SIL of the AP subsystem well.

To compare the performance of the proposed ALRF-LSTM and the conventional LSTM methods, three other updating methods were applied: 1) Stepwise, in which the initial learning rate was modified by multiplying by 0.1 at the 500th epoch; 2) Adam; and 3) ALRT, $\{U, S\} = \{3, [0.8, 1.0, 1.2]\}$. The initial learning rates for the three methods were set to 0.01, and the other model parameters were the same as in the ALRF-LSTM.

To analyze the overall performance of one model, Fig. 13 shows the MSE of the front wall SIL of the training and testing results of each sample. The MSE for the testing set was larger than that for the training set. The stepwise method had the largest testing MSE of 1.62 dB, and the MSE of Adam was 1.32 dB; the ALRT method had the relatively lower testing MSE of 1.17 dB, while the ALRF method obtained the lowest MSE of 1.00 dB. This is because the branch size and scale factor can adaptively adjust the learning rate during training, which makes the model find a better solution. Moreover, the beam space allows for the searching process to be more flexible and avoid local minima.

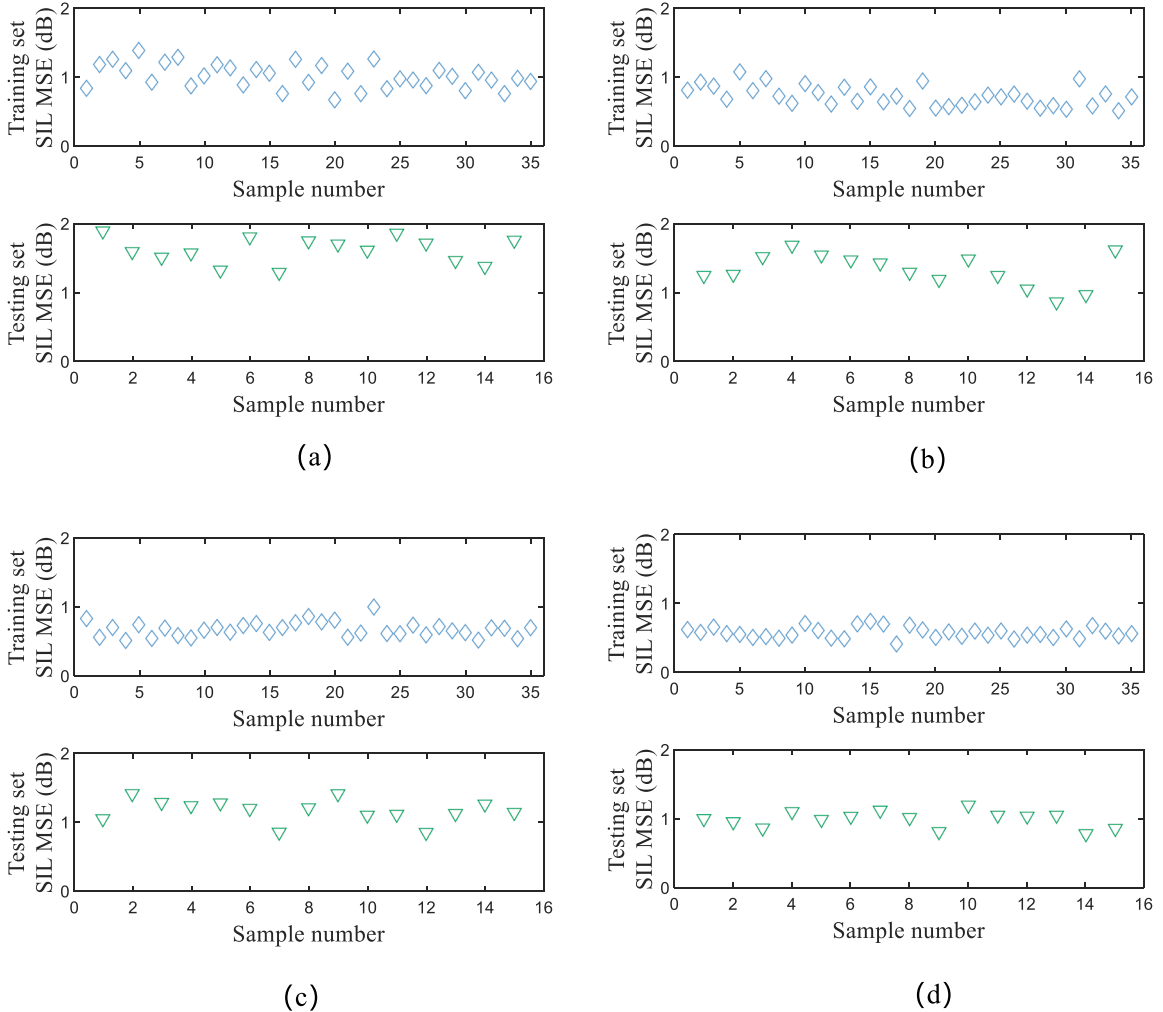


Fig. 13. MSE of LSTM with different updating methods. (a) Stepwise. (b) Adam. (c) ALRT, $\{U, S\} = \{3, [0.8, 1.0, 1.2]\}$. (d) ALRF, $\{U, S, V\} = \{3, [0.8, 1.0, 1.2], 3\}$.

To analyze the detailed performance of one model, Fig. 14 shows the relative error of the front wall SIL of the training and testing sets on the central frequency band. According to the maxima and minima as well as the first and third quartiles of the predicted relative error, the robustness of the stepwise, Adam, ALRT and ALRF methods gradually improved. In addition, the mean values of absolute error (MAE) of the stepwise, Adam, ALRT and ALRF methods were 6.56 %, 5.10 %, 4.87 % and 3.33 %, respectively; therefore, the accuracy of the four methods gradually increased. This means that the proposed ALRF-LSTM can predict the SIL of an AP system effectively.

To analyze the relationship between the learning rate and the training process, Fig. 15 shows the change in learning rate of the four methods. The learning rate of the stepwise method changed as predefined. The learning rate of Adam decreased gradually during training and then reached approximately 0.0022 at epoch 510. The learning rate of ALRT first increased at the peak of 5.61 and then fell to approximately 0.0007 at epoch 350 with fluctuation. Similarly, the learning rate of ALRF gradually increased with a large upper and lower span transition and reached the highest value of 7.96 at epoch 150. The peak learning rate was maintained for a few epochs and then decreased gradually as a solution was approached. This is because the beam space stores the previous noninferior solution and allows for the calculation process to jump out of the current local optimal solution. Fig. 16 shows the training loss of different methods. The Adam method obtained a better solution than the stepwise method, and the ALRF performed the best. It was found that adaptively adjusting the learning rate has two advantages: 1) a large learning rate at early epochs increases the efficiency of the training process and convergence speed; and 2) decreasing and increasing the learning rate adaptively can achieve the global optimum more effectively.

To investigate the influence of the parameters of ALRF-LSTM, several ALRF-LSTM models with different parameters were developed, and the testing results are presented in Table 1.

According to models #1, #2 and #3, the values of the scale factor influenced the training performance. When the preset upper and

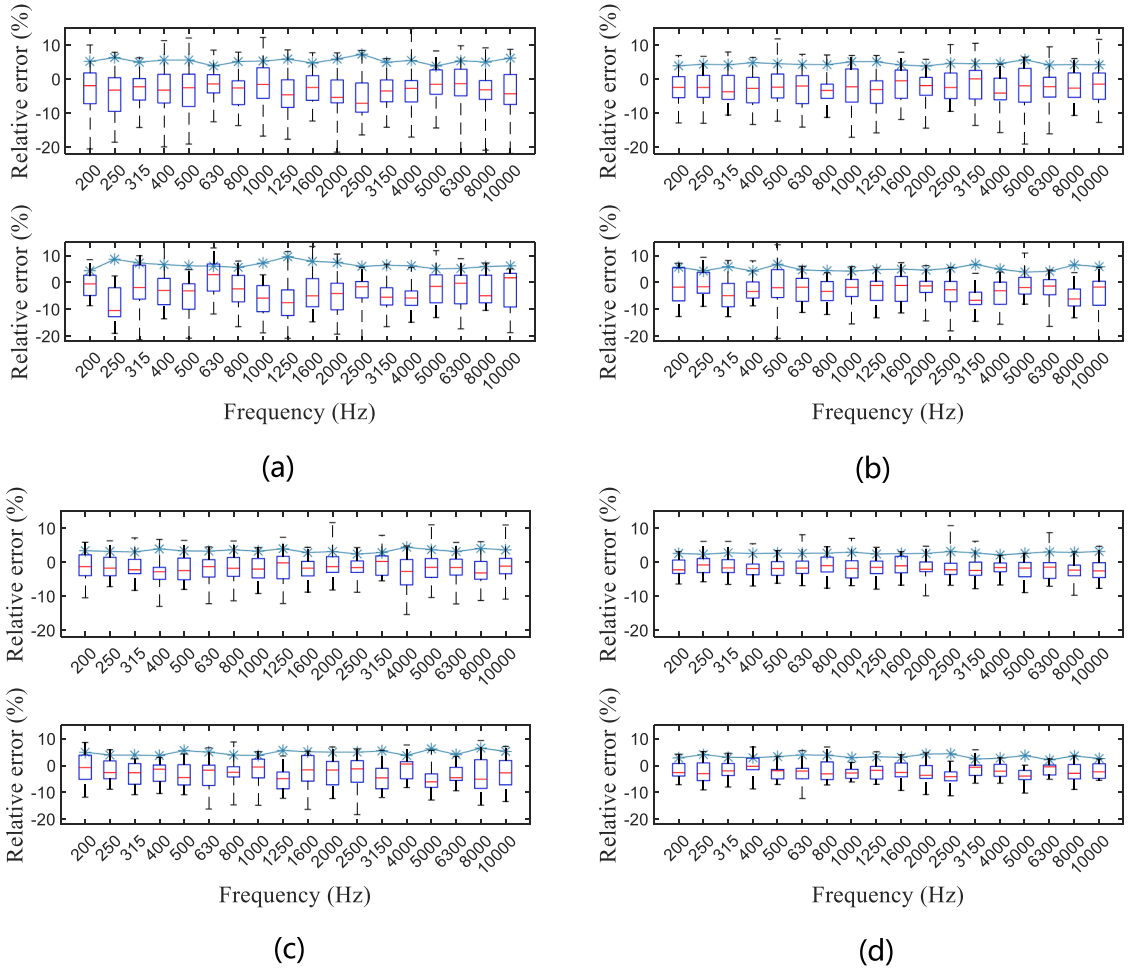


Fig. 14. Relative error of LSTM with different updating methods. (a) Stepwise. (b) Adam. (c) ALRT, $\{U, S\} = \{3, [0.8, 1.0, 1.2]\}$. (d) ALRF, $\{U, S, V\} = \{3, [0.8, 1.0, 1.2], 3\}$. The “ $-*$ ” is the mean value of the absolute error.

lower bounds of the scale factor narrowed ($[0.8, 1.2] \rightarrow [0.95, 1.05]$), the MSE of the front wall SIL increased from 1.00 dB to 1.12 dB, and the MAE and the standard deviation of error (STD) also increased to varying degrees. Therefore, a wide learning rate search range is more conducive to finding the optimal solution, but the degree of drastic changes in the learning rate needs to be controlled.

Comparing models #1, #4 and #5, the beam space affected the accuracy of the model. If the beam space is set to 1, the ALRF-LSTM becomes the ALRT-LSTM. When the values of beam space went from 1 to 6, the performance of the models greatly improved, with MSE of 1.17 dB and 0.93 dB, respectively. A large beam space can store more alternate calculation results; however, it increases the computation time and memory space. Therefore, the beam space should be large for high precision but small for low computational cost.

According to models #1, #6 and #7, a large branch size can offer more optional scale factors and make the model more flexible. Specifically, if the branch size, scale factor and beam space are all set to 1, the ALRF-LSTM corresponds to the conventional LSTM. Model #6 with branch number 5 outperformed model #1 with branch number 3 and obtained MSE, MAE and STD values of 0.92 dB, 2.91 % and 0.86 dB, respectively. However, when the branch number increased to 7, i.e., model #7, the MSE, MAE and STD were slightly better than those of model #6. This means that there was a lower limit on the testing error and that it could be achieved using a more appropriate branch number, such as 5, to save computational cost in this experiment. The study results indicate that the parameters of model #6 could balance the model effectiveness and efficiency.

To study the effect of the proposed mapping architecture, the SIL of the AP system was predicted through the traditional mapping method and the MLMO method. The traditional mapping method used the parameters of the component level as the ALRF-LSTM input and the STL of the AP system as the output, which neglected the characteristics of the subsystem level. In contrast, the MLMO method first used the parameters of the component level as the ALRF-LSTM[2] input and the SIL of the AP subsystem as the output and then applied the SIL of the subsystem as the ALRF-LSTM[1] input and the STL of the AP system as the output. Fig. 17 shows the predicted STL of the AP system via the two methods. The global trend and local trend of the predicted STL of the AP system using the MLMO method are better than those of the traditional mapping method.

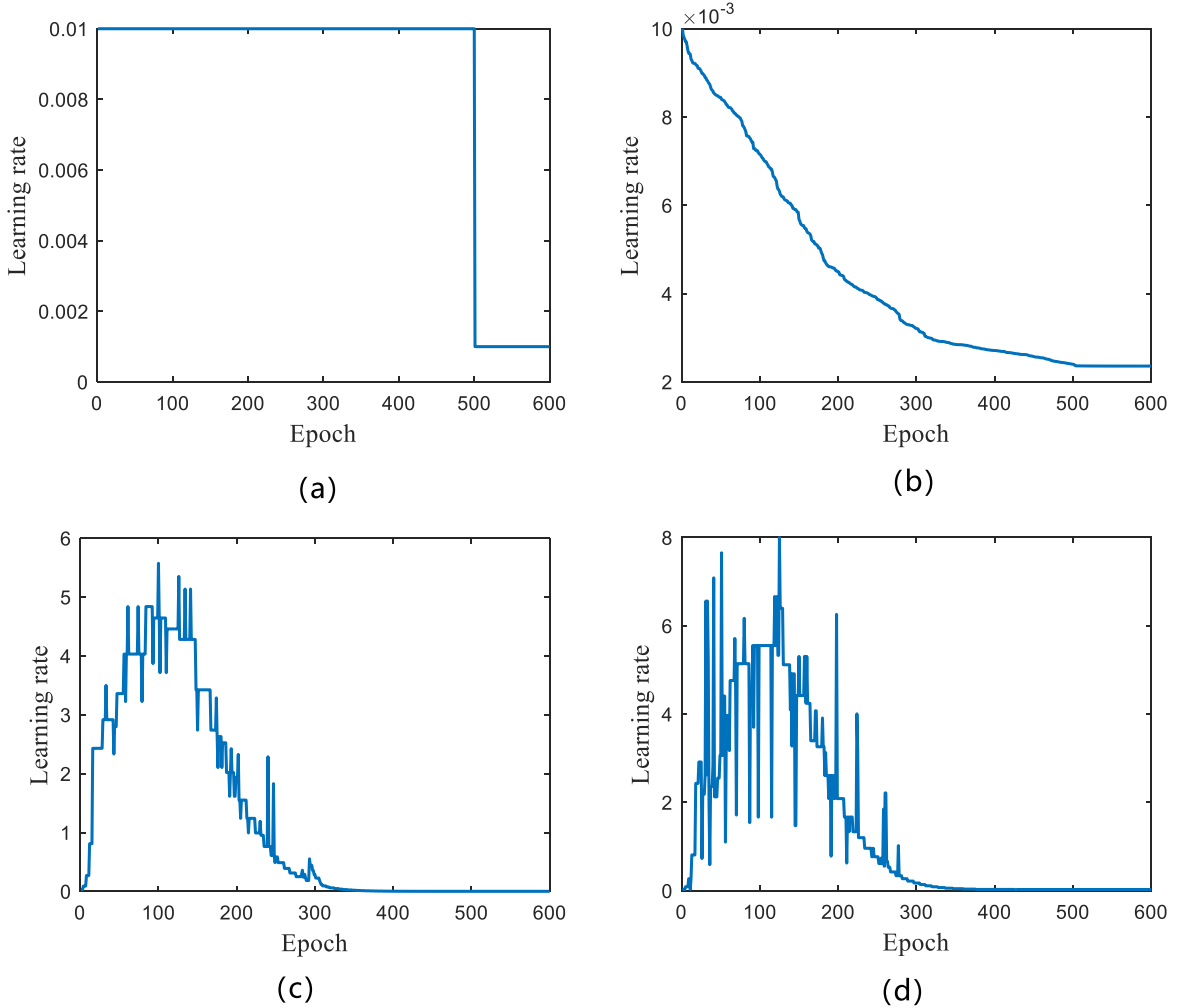


Fig. 15. Learning rate of LSTM with different updating methods. (a) Stepwise. (b) Adam. (c) ALRT, $\{U, S\} = \{3, [0.8, 1.0, 1.2]\}$. (d) ALRF, $\{U, S, V\} = \{3, [0.8, 1.0, 1.2], 3\}$.

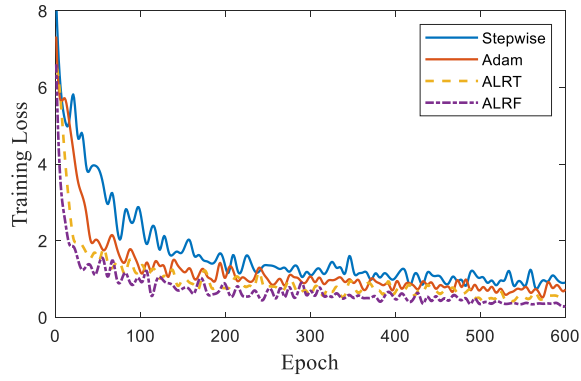


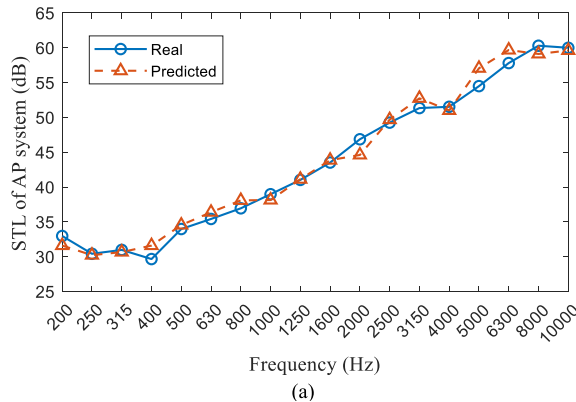
Fig. 16. Experimental results of ALRT-LSTM using different updating methods.

Table 2 presents the error analysis of the two methods. The MSE, MAE and STD of the AP system using the traditional mapping method were 1.57 dB, 4.9 % and 2.15 dB, respectively, while those of the AP system using the MLMO method were 1.12 dB, 2.77 % and 1.01 dB, respectively. Therefore, the comprehensive effectiveness of the MLMO architecture outperformed the traditional mapping method. In addition, in the MLMO method, the SIL of the AP subsystems also obtained good predicted results, and the maximum MAE

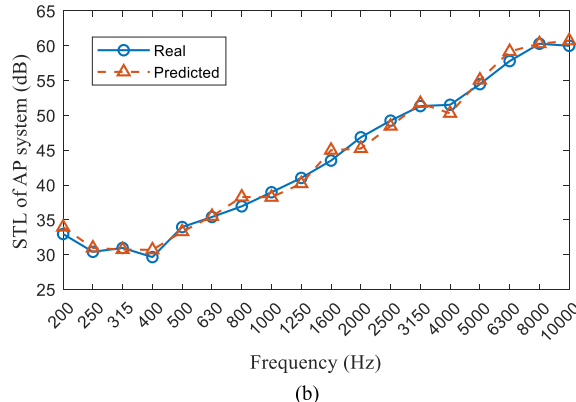
Table 1

Influence analysis of ALRF-LSTM model parameters on the testing set of the front wall.

No.	Parameters	MSE (dB)	MAE (%)	STD (dB)
#1	ALRF, $\{M, S, B\} = \{3, [0.8, 1.0, 1.2], 3\}$	1.00	3.33	0.94
#2	ALRF, $\{M, S, B\} = \{3, [0.9, 1.0, 1.1], 3\}$	1.08	4.12	1.09
#3	ALRF, $\{M, S, B\} = \{3, [0.95, 1.0, 1.05], 3\}$	1.12	4.41	1.15
#4	ALRF, $\{M, S, B\} = \{3, [0.8, 1.0, 1.2], 1\}$	1.17	4.87	1.28
#5	ALRF, $\{M, S, B\} = \{3, [0.8, 1.0, 1.2], 6\}$	0.93	2.96	0.84
#6	ALRF, $\{M, S, B\} = \{5, [0.8, 0.9, 1.0, 1.1, 1.2], 3\}$	0.92	2.91	0.86
#7	ALRF, $\{M, S, B\} = \{7, [0.8, 0.9, 0.95, 1.0, 1.05, 1.1, 1.2], 3\}$	0.91	2.86	0.84



(a)



(b)

Fig. 17. The predicted SIL of the AP system using ALRF-LSTM. (a) The traditional mapping method. (b) The MLMO method.**Table 2**

Comparison of the traditional and proposed mapping architectures.

Mapping architecture	MSE (dB)	MAE (%)	STD (dB)
Traditional mapping method STL of the AP system (ALRF –LSTM)	1.57	4.90	2.15
MLMO method STL of the AP system (ALRF – LSTM ₁ ^[1])	1.12	2.77	1.01
SIL of the front wall subsystem (ALRF – LSTM ₁ ^[2])	0.92	2.91	0.86
SIL of the dashboard subsystem (ALRF – LSTM ₂ ^[2])	0.75	2.82	0.92
SIL of the floor subsystem (ALRF – LSTM ₃ ^[2])	0.29	2.67	0.83
SIL of the door trim subsystem (ALRF – LSTM ₄ ^[2])	0.14	3.01	1.10
SIL of the roof trim subsystem (ALRF – LSTM ₅ ^[2])	0.24	2.85	0.95

and STD were 3.01 % and 1.10 dB, respectively. There are differences among the predicted MSE values of each AP subsystem because the overall SIL of each AP subsystem is different. The existence of the AP subsystem level in the MLMO structure reduces the nonlinear characteristic of the AP system. Compared with the traditional mapping method, the complex high-dimensional acoustic problem is decomposed into multiple low-dimensional acoustic problems, which simplifies the solution difficulty and improves the calculation

Table 3

Optimization results of the SIL of the AP system.

Methods	Design objectives	
Original status	Mean STL	43.63 dB
	STL curve in 1/3 Octave	[32.97, 30.41, 30.97, 29.66, 33.97, 35.41, 36.94, 38.97, 41.02, 43.52, 46.86, 49.25, 51.34, 51.53, 54.49, 57.80, 60.29, 60.00] dB
	Mean STL	44.71 dB
Traditional mapping method	STL curve in 1/3 Octave	[32.59, 31.40, 31.58, 30.91, 35.23, 37.27, 38.84, 39.23, 42.50, 43.33, 46.04, 51.20, 52.37, 52.47, 57.35, 59.47, 61.07, 61.93] dB
	Mean STL	45.72 dB
	STL curve in 1/3 Octave	[34.26, 31.27, 32.91, 30.61, 35.98, 35.14, 40.27, 42.01, 43.98, 46.97, 48.37, 52.10, 54.08, 54.01, 57.60, 58.81, 62.69, 61.90] dB
MLMO method		

Table 4

Optimization results of the AP component parameters.

Method	Design parameters				
	Front wall		Dashboard	Floor	Door trim
	$\{x_1^{[3]} - x_6^{[3]}\}^*$	$\{x_7^{[3]} - x_{10}^{[3]}\}^*$	$\{x_{11}^{[3]} - x_{16}^{[3]}\}^*$	$\{x_{17}^{[3]} - x_{20}^{[3]}\}^*$	$\{x_{21}^{[3]} - x_{26}^{[3]}\}^*$
Original state	{Glass cotton, EVA pad, PE pad, 30.0 mm, 2.5 mm, 1.5 mm}	{Felt, PU pad, 15.0 mm, 2.5 mm}	{Felt, HMP pad, PET pad, 22.5 mm, 2.5 mm, 2.0 mm}	{Felt, PU pad, 20.0 mm, 1.0 mm}	{Glass cotton, PU pad, PET pad, 25.0 mm, 2.5 mm, 2.0 mm}
Traditional mapping method	{Glass cotton, EVA pad, PU pad, 28.0 mm, 2.5 mm, 2.0 mm}	{Felt, PU pad, 12.0 mm, 3.0 mm}	{Felt, HMP pad, PE pad, 22.0 mm, 2.0 mm, 2.5 mm}	{Felt, PU pad, 20.0 mm, 1.0 mm}	{Felt, PU pad, PET pad, 27.0 mm, 2.0 mm, 2.0 mm}
MLMO method	{Glass cotton, EVA pad, PE pad, 30.0 mm, 3.0 mm, 2.0 mm}	{Glass cotton, PU pad, 20.0 mm, 1.5 mm}	{Felt, HMP pad, PET pad, 20.0 mm, 2.5 mm, 2.5 mm}	{Felt, PU pad, 18.0 mm, 1.5 mm}	{Felt, PE pad, PET pad, 23.0 mm, 2.5 mm, 3.0 mm}

* The subscripts of design parameters $\{x_1^{[3]} - x_{26}^{[3]}\}$ are corresponded to the sound absorption and insulation material types and thicknesses shown in Fig. 6.

accuracy.

5.3. Optimization of AP performance

Prediction can be thought of as a forward design process, while optimization can be thought of as a reverse design process. The proposed ALRF-LSTM method and the MLMO method were used to optimize the SAI performance of the AP system. According to the MLMO structure, the STL of the AP system (design objective) is influenced by multiple SILs of the AP subsystem (design parameters) in the lower level, and the SIL of the AP subsystem (design objective) is affected by multiple SILs of the AP component in the lower level that is connected to it. Therefore, the layerwise optimization model to optimize the SAI of the AP system is defined as follows:

Table 5
Conditions of the optimization model.

Method	Constraints	
	W(kg)	C(CNY)
Original state	61.5	14,100
Traditional mapping method	61.2	14,090
MLMO method	61.4	14,077

$$\begin{aligned}
 \min \quad & \{y_1^{[1]}(y_1^{[2]}, y_2^{[2]}, y_3^{[2]}, y_4^{[2]}, y_5^{[2]})\} \\
 & y_1^{[1]} = f_1^{[1]}(y_1^{[2]}, y_2^{[2]}, y_3^{[2]}, y_4^{[2]}, y_5^{[2]}) \\
 & y_1^{[2]} = f_1^{[2]}(x_1^{[3]}, x_2^{[3]}, x_3^{[3]}, x_4^{[3]}, x_5^{[3]}, x_6^{[3]}) \\
 & y_2^{[2]} = f_2^{[2]}(x_7^{[3]}, x_8^{[3]}, x_9^{[3]}, x_{10}^{[3]}) \\
 & y_3^{[2]} = f_3^{[2]}(x_{11}^{[3]}, x_{12}^{[3]}, x_{13}^{[3]}, x_{14}^{[3]}, x_{15}^{[3]}, x_{16}^{[3]}) \\
 & y_4^{[2]} = f_4^{[2]}(x_{17}^{[3]}, x_{18}^{[3]}, x_{19}^{[3]}, x_{20}^{[3]}) \\
 & y_5^{[2]} = f_5^{[2]}(x_{21}^{[3]}, x_{22}^{[3]}, x_{23}^{[3]}, x_{24}^{[3]}, x_{25}^{[3]}, x_{26}^{[3]}) \\
 \text{s. t.} \quad & W = \sum_{i=1}^{26} \delta_i \times s_i \times \rho_i \leq W_0 \\
 & C = \sum_{i=1}^{26} \delta_i \times s_i \times \rho_i \times p_i \leq C_0 \\
 \text{var.} \quad & x_1^{[3]}, x_7^{[3]}, x_{11}^{[3]}, x_{17}^{[3]}, x_{21}^{[3]} \in \{\text{SILGlass, cotton, SILFelt}\} \\
 & x_2^{[3]}, x_3^{[3]}, x_8^{[3]}, x_{12}^{[3]}, x_{13}^{[3]}, x_{18}^{[3]}, x_{22}^{[3]}, x_{23}^{[3]} \in \{\text{SILEVA, SILPE Pad, SILPU Pad, SILHMP Pad, SILPET Pad}\} \\
 & x_4^{[3]}, x_9^{[3]}, x_{14}^{[3]}, x_{19}^{[3]}, x_{24}^{[3]} \in [5.0, 40.0] \\
 & x_5^{[3]}, x_6^{[3]}, x_{10}^{[3]}, x_{15}^{[3]}, x_{16}^{[3]}, x_{20}^{[3]}, x_{25}^{[3]}, x_{26}^{[3]} \in [1.0, 10.0]
 \end{aligned} \tag{7}$$

where $y_1^{[1]}$ is the STL curve of the AP system and $y_1^{[2]}, y_2^{[2]}, y_3^{[2]}, y_4^{[2]}, y_5^{[2]}$ are the SIL curves of the AP subsystems, i.e., the SIL of the front wall, dashboard, floor, door trim, and roof trim, respectively. f is the accordingly developed ALRF-LSTM model. W and C are the constraints of the weight and cost of the AP system, respectively, and W_0 and C_0 are the weight and cost of the AP original status, with values of 61.5 kg and 14100CNY, respectively. δ represents the thickness, s represents the square, ρ represents the material density and p represents the unit price. The square of each component was predetermined according to the vehicle type, and the density of the SAI materials and unit price were obtained from the database of Changan Auto Global R&D Center, Chongqing Changan Automobile Co., Ltd, China. $x_1^{[3]} - x_{26}^{[3]}$ are design parameters of the AP components, which are related to the SAI material type and thickness, and their subscript denotes the parameter serial number in Fig. 6.

The design vector of the objective function was calculated and optimized through the genetic algorithm (GA). The population size, crossover rate and mutation rate of the GA were set as 300, 0.6 and 0.05, respectively. The stopping criterion was imposed to limit the GA run to a maximum of 500 generations. The GA parameters for the traditional mapping method and the MLMO method were identical. Tables 3–5 show the optimization results of the AP system.

As listed in Table 3, the optimized mean STL via the traditional mapping method was 44.71 dB, which is 1.08 dB higher than that of the original status; however, the optimized mean STL of the MLMO method is 2.09 dB higher than that of the original status and was 45.72 dB. Through the 1/3 octave band,¹ the development of the STL concentrated within the frequency of [500, 10000] Hz.

In Table 4, the material type and the corresponding thickness of the AP components have been optimized. Through the traditional mapping method, the 2nd layer material type of the cabin side of the front wall was modified from PE pad to PU pad, its thickness was increased to 2.0 mm, and the thickness of the glass cotton was reduced from 30.0 mm to 28.0 mm. For the dashboard, the thicknesses of the felt and PU pad were modified from 15.0 mm and 2.5 mm to 20.0 mm and 3.0 mm, respectively. In addition, the design parameters of floor, door trim and roof trim were optimized, and are italicized in Table 4. In contrast, through the MLMO method, the thicknesses of the EVA pad and PE pad increased to 3.0 mm and 2.0 mm, respectively. The material type of the powertrain side of the dashboard was modified from felt to glass cotton, and the thickness increased by 5.0 mm. Meanwhile, the thickness of the PU pad was reduced to 1.5 mm. Other parameters of AP components are also italicized. Both methods satisfied the constraint condition according to Table 5.

Based on the above study, the traditional mapping method uses all design parameters to construct the optimization model, resulting in high model complexity and strong nonlinearity. However, using the MLMO method, the nonlinearity of the AP system is decomposed into several submodels, which reduces the complexity of the solution and is more conducive to the optimization analysis of the problem.

¹ 1/3 Octave band: [200, 250, 315, 400, 500, 630, 800, 1000, 1250, 1600, 2000, 2500, 3150, 4000, 5000, 6300, 8000, 10000] Hz.

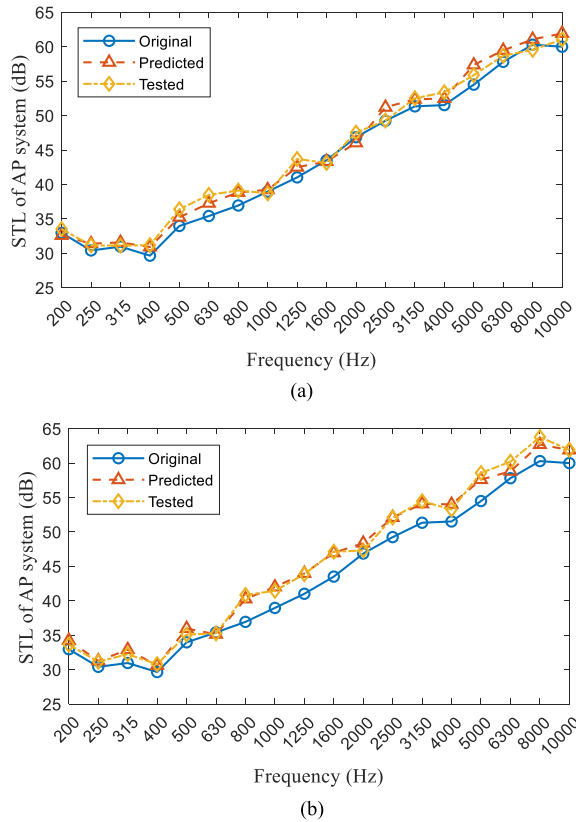


Fig. 18. Comparison of the predicted and tested SIL of the AP system. (a) The traditional mapping method. (b) The MLMO method.

Table 6

The tested error of the STL of the AP system using different optimization methods.

Method	Error statistics between the optimized and tested conditions	
Traditional mapping method	Mean absolute error of the STL	1.93 %
	Relative error of the SIL curve in 1/3 Octave	[2.85, -0.8, -1.46, 0.87, 3.29, 3.27, 0.72, -1.35, 2.82, -0.46, 3.24, -3.73, 0.27, 1.73, -2.56, -1.31, -2.51, -1.42] %
	Octave	
MLMO method	Mean absolute error of the STL	1.17 %
	Relative error of the SIL curve in 1/3 Octave	[-1.84, -0.32, -2.04, 0.59, -2.45, 0.37, 1.44, -1.33, -0.25, 0.34, -2.19, -0.02, 0.7, -1.39, 1.68, 2.36, 1.74, 0.03] %
	Octave	

5.4. Experiment validation

To validate the proposed method and the optimized results, the AP systems constituted by the AP components presented in Table 4 were applied, and a vehicle test was implemented. The working condition and the experimental environment were the same as those in Section 4. The tested STLs of the AP system using the traditional mapping method and the MLMO method are shown in Fig. 18. The actual performance of the modified AP system was improved and approximated the optimized result.

Table 6 shows the error statistics between the optimized and tested STL of the AP system. The mean absolute errors of the tested STL of the traditional mapping method and the MLMO method between the optimized and tested conditions were 1.93 % and 1.17 %, respectively, which illustrates that the MLMO method has better robustness. In addition, the maximum and minimum errors of the relative error of the STL curve in 1/3 Octave were 3.29 % (500 Hz) and -3.73 % (2500 Hz) for the traditional mapping method and 2.36 % (6300 Hz) and -2.45 % (500 Hz) for the MLMO method. This shows that the MLMO method also has better accuracy in practice than the traditional mapping method.

6. Conclusion

In this paper, we re-examine traditional data-driven methods from the perspective of noise transfer relationships and hierarchical target decomposition of AP systems of EVs. The SAI of the AP system was predicted and optimized through the proposed knowledge-

and data-driven approach, which is composed of the ALRF-LSTM method and the MLMO method. The ALRF-LSTM is able to decrease and increase the learning rate adaptively in accordance with the training loss, obtaining predicted MSE, MAE and STD of the STL of the AP system of 1.12 dB, 2.77 % and 1.01 dB, respectively, which is better than those of the traditional mapping method of 1.57 dB, 4.9 % and 2.15 dB. In addition, the proposed MLMO structure can reduce the complexity of the problem via decomposition of the AP system, subsystem, and component levels. The optimized mean STL of the AP system via the MLMO method was 45.72 dB, which is 1.01 dB higher than that of the traditional mapping method. Furthermore, the effectiveness and robustness of the MLMO method was validated through a vehicle experiment.

Declaration of Competing Interest

The authors declare that they have no known competing financial interests or personal relationships that could have appeared to influence the work reported in this paper.

Data availability

The authors do not have permission to share data.

Acknowledgments

This work was supported by the National Natural Science Foundation of China (No. 51905408), the SWJTU Science and Technology Innovation Project (2682022CX008, 2682021ZTPY068), the Vehicle Measurement, Control and Safety Key Laboratory of Sichuan Province Project (QCCK2022-002), and the Fund of State Key Laboratory of Vehicle NVH and Safety Technology (NVHSKL-202203).

Appendix A

Abbreviations

Adam	Adaptive Moment Estimation Adam
ALRF	Adaptive learning rate forest
ALRF-LSTM	Long short-term memory based on adaptive learning rate forest
ALRT	Adaptive learning rate tree
AP	Acoustic package
CNN	Convolutional neural network
EV	Electric vehicle
EVA	Ethylene vinyl acetate copolymer
FE-SEA	Finite element-statistical energy analysis
HMP	High molecular polymer
LHD	Latin hypercube design
LSTM	Long short-term memory
MAE	Mean values of absolute error
MLMO	Multiple-level multiple-object
MSE	mMean square error
NN	Neural network
NVH	Noise, vibration and harshness
PE	Polyethene
PET	Polyethylene terephthalate
PU	Polyurethane
SAI	Sound absorption and insulation
SEA	Statistical energy analysis
SIL	Sound isolation loss
SPL	Sound pressure level

References

- [1] G. Long, Y. Wang, T.C. Lim, Optimal parametric design of delayless subband active noise control system based on genetic algorithm optimization, *J. Vib. Control* 28 (15–16) (2022) 1950–1961.
- [2] X. Wang, X.F. Geng, X.Y. Mao, H. Ding, X.J. Jing, L.Q. Chen, Theoretical and experimental analysis of vibration reduction for piecewise linear system by nonlinear energy sink, *Mech. Syst. Sig. Process.* 172 (2022), 109001.
- [3] H.B. Huang, X.R. Huang, M.L. Yang, T.C. Lim, W.P. Ding, Identification of vehicle interior noise sources based on wavelet transform and partial coherence analysis, *Mech. Syst. Sig. Process.* 109 (2018) 247–267.
- [4] J. Pang, Noise and vibration control in automotive bodies, John Wiley & Sons, 2018.
- [5] N. Gao, M. Wang, B. Cheng, H. Hou, Inverse design and experimental verification of an acoustic sink based on machine learning, *Appl. Acoust.* 180 (2021), 108153.

- [6] J. Zhang, J. Pang, Y. Wan, L. Yang, W. Jia, Zhang, S Analysis of Structure-Acoustic Coupling Characteristics Between Adjacent Flexible Panels and Enclosed Cavity, *J. Vib. Acoust.* 143 (2) (2021), 021006.
- [7] G. Petrone, G. Melillo, A. Laudiero, S. De Rosa, A Statistical Energy Analysis (SEA) model of a fuselage section for the prediction of the internal Sound Pressure Level (SPL) at cruise flight conditions, *Aerosp. Sci. Technol.* 88 (2019) 340–349.
- [8] H.R. Lee, H.Y. Kim, J.H. Jeon, Y.J. Kang, Application of global sensitivity analysis to statistical energy analysis: Vehicle model development and transmission path contribution, *Appl. Acoust.* 146 (2019) 368–389.
- [9] H. Li, D. Thompson, G. Squicciarini, X. Liu, M. Rissmann, P. Bouvet, J.M. García-Loygorri, A framework to predict the airborne noise inside railway vehicles with application to rolling noise, *Appl. Acoust.* 179 (2021), 108064.
- [10] Q. Liu, D.J. Thompson, P. Xu, Q. Feng, X. Li, Investigation of train-induced vibration and noise from a steel-concrete composite railway bridge using a hybrid finite element-statistical energy analysis method, *J. Sound Vib.* 471 (2020), 115197.
- [11] Z. Mohamed, X. Wang, A deterministic and statistical energy analysis of tyre cavity resonance noise, *Mech. Syst. Sig. Process.* 70 (2016) 947–957.
- [12] L. Yu, X. Gu, L. Qian, P. Jiang, W. Wang, M. Yu, Application of tailor rolled blanks in optimum design of pure electric vehicle crashworthiness and lightweight, *Thin-Walled Structures* 161 (2021), 107410.
- [13] C.W. Hudson, J.J. Carruthers, A.M. Robinson, Multiple objective optimisation of composite sandwich structures for rail vehicle floor panels, *Compos. Struct.* 92 (9) (2010) 2077–2082.
- [14] Nam, G. H., Bu, S. J., Park, N. M., Seo, J. Y., Jo, H. C., Jeong, W. T. Data augmentation using empirical mode decomposition on neural networks to classify impact noise in vehicle. In ICASSP 2020-2020 IEEE International Conference on Acoustics, Speech and Signal Processing (ICASSP) (2020, May, pp. 731-735). IEEE.
- [15] M.A. Hannan, D.N. How, M.H. Lipu, P.J. Ker, Z.Y. Dong, M. Mansur, F. Blaabjerg, SOC estimation of li-ion batteries with learning rate-optimized deep fully convolutional network, *IEEE Trans. Power Electron.* 36 (7) (2020) 7349–7353.
- [16] G. Vrbančić, V. Podgorelec, Efficient ensemble for image-based identification of Pneumonia utilizing deep CNN and SGD with warm restarts, *Expert Syst. Appl.* 187 (2022), 115834.
- [17] Schaul, T., Zhang, S., LeCun, Y. No more pesky learning rates. In International Conference on Machine Learning (2013, May, pp. 343-351). PMLR.
- [18] C. Yu, X. Qi, H. Ma, X. He, C. Wang, Y. Zhao, LLR: Learning learning rates by LSTM for training neural networks, *Neurocomputing* 394 (2020) 41–50.
- [19] H. Huang, J. Wu, T.C. Lim, M. Yang, W. Ding, Pure electric vehicle nonstationary interior sound quality prediction based on deep CNNs with an adaptable learning rate tree, *Mech. Syst. Sig. Process.* 148 (2021), 107170.
- [20] S. Ye, J. Zhang, B. Xu, L. Hou, J. Xiang, H. Tang, A theoretical dynamic model to study the vibration response characteristics of an axial piston pump, *Mech. Syst. Sig. Process.* 150 (2021), 107237.
- [21] H.B. Huang, J.H. Wu, X.R. Huang, M.L. Yang, W.P. Ding, A generalized inverse cascade method to identify and optimize vehicle interior noise sources, *J. Sound Vib.* 467 (2020), 115062.
- [22] Ambardekar, M., Solanki, N. Performance cascading from vehicle-level NVH to component or sub-system level design. *SAE International Journal of Vehicle Dynamics, Stability, and NVH*, 1(2017-26-0205), 58-65.
- [23] Wu, W., Ding, P., Zi, X., Liu, B. An Acoustic Target Setting and Cascading Method for Vehicle Trim Part Design (No. 2019-01-1581). SAE Technical Paper.
- [24] Bergen, B., Schaefer, N., Van de Rostyne, K., Keppens, T. Vehicle Acoustic Performance Analysis towards Effective Sound Package Design in Mid-Frequency (No. 2018-01-1495). SAE Technical Paper.
- [25] N.G.R. de Melo Filho, L. Van Belle, C. Claeys, E. Deckers, W. Desmet, Dynamic mass based sound transmission loss prediction of vibro-acoustic metamaterial double panels applied to the mass-air-mass resonance, *J. Sound Vib.* 442 (2019) 28–44.
- [26] Y. Yu, X. Si, C. Hu, J. Zhang, A review of recurrent neural networks: LSTM cells and network architectures, *Neural Comput.* 31 (7) (2019) 1235–1270.
- [27] Pascanu, R., Mikolov, T., Bengio, Y. On the difficulty of training recurrent neural networks. In International conference on machine learning (2013, May, pp. 1310-1318). PMLR.
- [28] A. Sagheer, M. Kotb, Time series forecasting of petroleum production using deep LSTM recurrent networks, *Neurocomputing* 323 (2019) 203–213.
- [29] M. Abdel-Nasser, K. Mahmoud, Accurate photovoltaic power forecasting models using deep LSTM-RNN, *Neural Comput. Appl.* 31 (7) (2019) 2727–2740.
- [30] Wang, H., Li, C., Tachon, T., Wang, H., Yang, S., Limet, S., Robert, S. Efficient and Systematic Partitioning of Large and Deep Neural Networks for Parallelization. In European Conference on Parallel Processing (2021, September, pp. 201-216). Springer, Cham.
- [31] ISO 10534-2 Acoustics — Determination of properties in impedance tubes.
- [32] O. Doutres, N. Atalla, Experimental estimation of the transmission loss contributions of a sound package placed in a double wall structure, *Appl. Acoust.* 72 (6) (2011) 372–379.
- [33] Y.S. Wang, N.N. Liu, H. Guo, X.L. Wang, An engine-fault-diagnosis system based on sound intensity analysis and wavelet packet pre-processing neural network, *Eng. Appl. Artif. Intell.* 94 (2020), 103765.
- [34] SAE J1400-2017: Laboratory Measurement of the Airborne Sound Barrier Performance. 2017, SAE international.
- [35] GB/T 18697-2002: Acoustics – Method for Measuring the Vehicle Interior Noise, 2002.
- [36] GB/T 6881.2-2017:Acoustics – Acoustics—Determination of sound power levels and sound energy levels of noise sources using sound pressure—Engineering methods for small movable sources in reverberant fields—Comparison method for a hard-walled test room.
- [37] X. Wang, Y. Chen, G. Zhou, T. Chen, F. Ma, Synergetic coupling large-scale plate-type acoustic metamaterial panel for broadband sound insulation, *J. Sound Vib.* 459 (2019), 114867.
- [38] H. Huang, X. Huang, W. Ding, M. Yang, D. Fan, J. Pang, Uncertainty optimization of pure electric vehicle interior tire/road noise comfort based on data-driven, *Mech. Syst. Sig. Process.* 165 (2022), 108300.
- [39] X. Zheng, W. Dai, Y. Qiu, Z. Hao, Prediction and energy contribution analysis of interior noise in a high-speed train based on modified energy finite element analysis, *Mech. Syst. Sig. Process.* 126 (2019) 439–457.
- [40] H. Huang, X. Huang, W. Ding, M. Yang, X. Yu, J. Pang, Vehicle interior vibro-acoustical comfort optimization using a multi-objective interval analysis method, *Expert Syst. Appl.* 119001 (2022).
- [41] M. Stender, M. Tiedemann, D. Spieler, D. Schoepflin, N. Hoffmann, S. Oberst, Deep learning for brake squeal: Brake noise detection, characterization and prediction, *Mech. Syst. Sig. Process.* 149 (2021), 107181.